[UCI]I804:21031-200000371987

Thesis for the Degree of Master of Engineering

Application and Effect of Organic Electrolytes for Polymer Solar Cells

by

Mijin Jeong

Department of Polymer Engineering

The Graduate School

Pukyong National University

February 2021

Application and Effect of Organic Electrolytes for Polymer Solar Cells
(고분자 태양전지의 효율 향상을 위한 유기 전해질의 적용 및 효과)

Adviser: Prof. Joo Hyun Kim

by
Mijin Jeong

A thesis submitted in partial fulfillment of the requirements
for the degree of

Master of Engineering

in Department of Polymer Engineering, The Graduate School,
Pukyong National University

February 2021

Application and Effect of Organic Electrolytes for Polymer Solar Cells

A dissertation
by
Mijin Jeong

Approved by:

(Chairman) Prof. Seong il Yoo

(Member) Prof. Mun Ho Kim

(Member) Prof. Joo Hyun Kim

February 19, 2021

Contents

Chapter Ⅱ Simple Small Molecular Electrolytes as the Interlayer for Inverted Polymer Solar Cells

Chapter Ⅲ Small Molecular Electrolyte Hybridized ZnO for Polymer Solar Cells without Thickness Limitation

List of Figures

List of Tables

고분자 태양전지의 효율 향상을 위한 유기 전해질의 적용 및 효과

정 미 진

부 경 대 학 교 대 학 원 고 분 자 공 학 과

요 약

최근 환경오염 및 화석 연료의 고갈 문제로 신재생 에너지 개발이 활발히 진행되고 있다. 대체 에너지원 가운데 태양전지는 유해물질이 발생하지 않고 유지비가 적다는 측면에서 우위를 선점하고 있다. 그 중 고분자 태양전지는 유연성 및 경량성이 뛰어나 웨어러블 태양전지에 사용되고 있으나 낮은 효율을 보인다는 단점이 있다. 이에 본 연구에서는 고분자 태양전지의 효율을 향상시키기 위하여 전자 수송층과 광활성층 사이에 음극 버퍼 중간층을 도입하였다. 전자 수송층으로 사용되는 산화아연은 무기물이며 광활성층으로는 주로 유기물이 사용된다. 따라서, 계면에 에너지 장벽이 생겨 전자의 이동 및 수집 능력이 저하된다. 이때 쌍극자 모멘트를 갖는 전해질을 중간층으로써 도입하게 되면 에너지 장벽이 감소되어 전자의 이동 및 수집이 쉬워지며 단락 전류가 증가한다. 이러한 효과를 위하여 쌍극자 모멘트를 갖는 전해질을 설계하였으며 배치 간의 분자량 차이가 없고 합성 및 정제가 쉬운 저분자 물질을 합성하였다. 먼저, C4-OH 및 C6-OH를 합성하여 알킬 길이의 차이에 의한 고분자 태양전지의 광전변환효율 변화를 확인하였다. 그리고 C6-E-OTs를 도입하여 음이온 크기의 차이에 의한 에너지 장벽의 감소 및 효율 변화를 확인하였다. C6-E-OTs를 이용하여 역구조 고분자 태양전지를 제조한 결과, C6-E-Br을 도입했을 때보다 높은 효율을 보여주었다. 하지만 고분자 태양전지에 C6-E-OTs를 중간층으로 도입하여 뛰어난 성능을 보여주어도 실제 산업 공정에는 적용할 수가 없다. 고분자 태양전지를 상용화하기 위해서는 roll-to-roll 공정이 필수적이다.

하지만 중간층을 도입할 경우 5 nm 이하의 박막을 유지해야 하기 때문에 roll-to-roll 공정에 제한이 생긴다. 이때 중간층에 사용되는 물질을 전자 수송층으로 사용되는 산화 아연과 혼합하여 제조함으로써 두께 의존성을 없앨 수 있다. 따라서, 가장 높은 효율을 보여준 C6-E-OTs를 이용하여 혼합 용액을 제조하여 고분자 태양전지에 도입하였다. 그 결과 중간층으로 도입했을 때보다 더 좋은 성능을 보여주었다. 결과적으로 유기 전해질인 C6-E-OTs를 도입하여 고분자 태양전지의 단점인 낮은 효율 측면을 보완할 수 있었으며 실제 산업 공정에도 적용이 가능하여 고분자 태양전지의 상용화에 기여할 수 있었다.

Chapter Ⅰ
Introduction

Ⅰ-ⅰ Motivation

Fossil fuel has been a representation of energy source for a long time. For those times, several environmental problems have emerged in many places such as environmental pollution, global warming and an increase of water temperature [1]. Thus, many clean energy systems have been developed to solve these problems. Many researchers tried to fabricate solar cells using solar energy as a candidate for a clean energy system [2]. Solar cells have many attractive advantages, which are renewable energies without chemical pollution, noise pollution and release of greenhouse-effect gases [3]. Moreover, solar cells have a cost-saving effect due to the direct conversion of sunlight to electricity, maintenance for a long time without repair and no escalating fuel cost problem [4].

Ⅰ-ii Polymer Solar Cells

There are many types of solar cells such as silicon solar cells [5], organic solar cells [6], polymer solar cells [7], perovskite solar cells [8], quantum dot solar cells [9] and dye-sensitized solar cells [10]. In the middle of these solar cells, polymer solar cells (PSCs) have attracted attention with many advantages.

Ⅰ-ii-1. Definition

Polymer solar cells are one part of organic solar cells that use organic materials such as polymers or organic small molecule for an active layer. PSCs use conductive polymers as a donor or acceptor in the active layer, which can absorb light and generate electricity by the photovoltaic effect [11].

Ⅰ-ⅱ-2. Advantages

PSCs have many advantages such as lightweight, mechanical flexibility, solution process and low-cost process [12]. Thus, PSCs can be applied to flexible solar cells and wearable solar cells due to their light and flexible properties [13]. Furthermore, the roll-to-roll process is possible because the solution process is possible [14]. The light absorption region can also be adjusted by controlling the band gap by modifying the donor and the acceptor used as an active layer [15].

Ⅰ-ⅱ-3. Disadvantages

On the other hand, PSCs also have disadvantages. PSCs still show low efficiencies for commercial use. Moreover, PSCs have low stability for long term use and low strength. Therefore, the current research direction of PSCs is focused on efficiency improvement and stability [16].

Ⅰ-ⅱ-4. Principle of PSCs

PSCs are operated by four main steps, which are exciton generation, exciton diffusion, charge separation and charge collection (shown in **Figure Ⅰ-1**) [17].

PSCs consist of a junction structure with an electron donor and an electron acceptor forming an active layer. When light is examined in PSCs, exciton, a pair of electron and hole, is formed in the electron donor [18]. Because the formed exciton has a very short lifetime of few picoseconds, the exciton diffusion is limited to less than 20 nm [19]. As a result, the exciton at the interface between the donor and the acceptor is dissociated to the electron and hole. This mechanism occurs effectively due to an acceptor that pulls the electron strongly. Separated electron and hole are collected to cathode and anode, respectively [20].

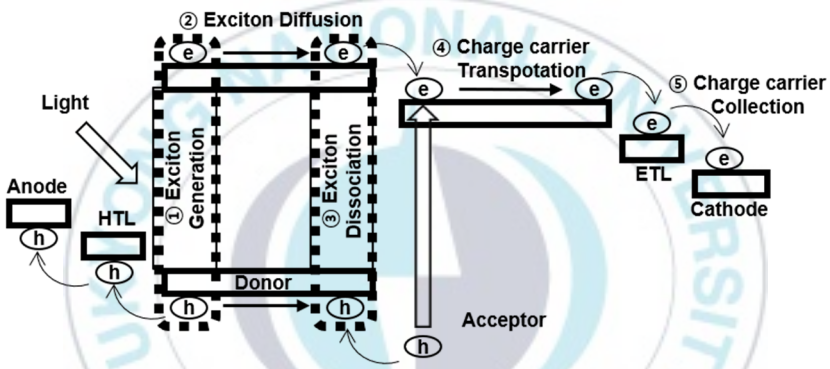

Figure Ⅰ**- 2** Operating mechanism of PSCs.

Ⅰ-ⅱ-5. Architecture of PSCs

The architecture of PSCs is largely classified as the conventional type and the inverted type (shown in **Figure Ⅰ- 2**). Conventional PSCs consist of a [anode/hole transport layer (HTL)/active layer/electron transport layer (ETL)/cathode] [21]. PEDOT:PSS is commonly used as HTL, which is acidic and thus adversely affects the long-term stability of PSCs [22]. Inverted PSCs (iPSCs) were introduced to overcome the limitation of stability. IPSCs consist of [cathode/ETL/active layer/HTL/anode] [23]. In this case, the ZnO layer is used as ETL, which is not acidity and thus can develop the stability of PSCs [24].

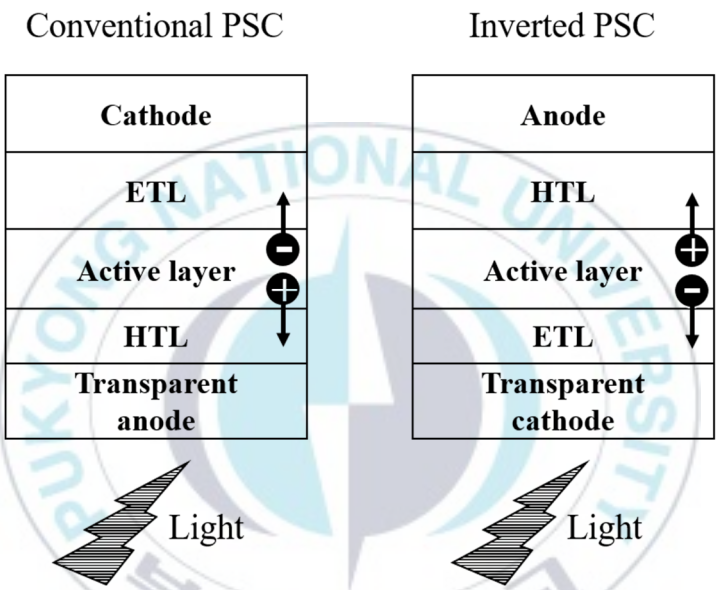

Figure Ⅰ - 2 Device architectures of conventional and inverted PSC.

For this reason, iPSCs were researched in this paper, which were fabricated with ITO as the cathode, ZnO as ETL, blend of PTB7 or PTB7-Th and $PC_{71}BM$ as the active layer, MoO_3 as HTL and Ag as the anode (shown in **Figure Ⅰ - 3**).

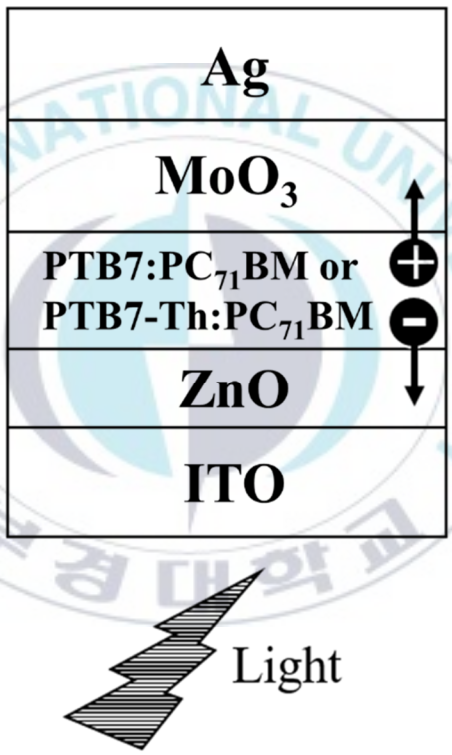

Figure Ⅰ - 3 Device architecture of iPSC used in this research.

Ⅰ-ⅱ-6. Cathode Interlayer

Between the ZnO layer and the active layer, there will be a potential energy barrier for electrons generated at a metal-semiconductor junction [25]. At this time, Schottky barrier height (Φ_B) is an essential factor, and this depends on the combination of metal and semiconductor (shown in **Figure Ⅰ- 4**) [26]. The metal-semiconductor junction, in which Φ_B is too low to conduct current in all directions without rectification characteristics, is called ohmic contact [27]. IPSC is hard to reach ohmic contact due to the intrinsic properties of the semiconductor [28]. However, a cathode interlayer can be introduced between ZnO and the active layer to reduce Schottky barrier height [29]. This cathode interlayer is usually formed with electrolytes, resulting in an interface dipole between the ZnO and active layer layers (shown in **Figure Ⅰ- 5**) [30]. As a result, the Schottky barrier height can be reduced and the current can be increased.

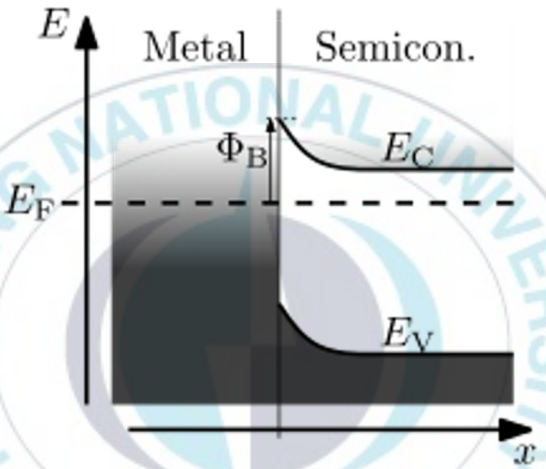

Figure Ⅰ - 4 Band diagram for metal-semiconductor junction (Φ_B: Schottky barrier height, E_C: conduction band edge, E_V: valence band edge and E_F: Fermi level)

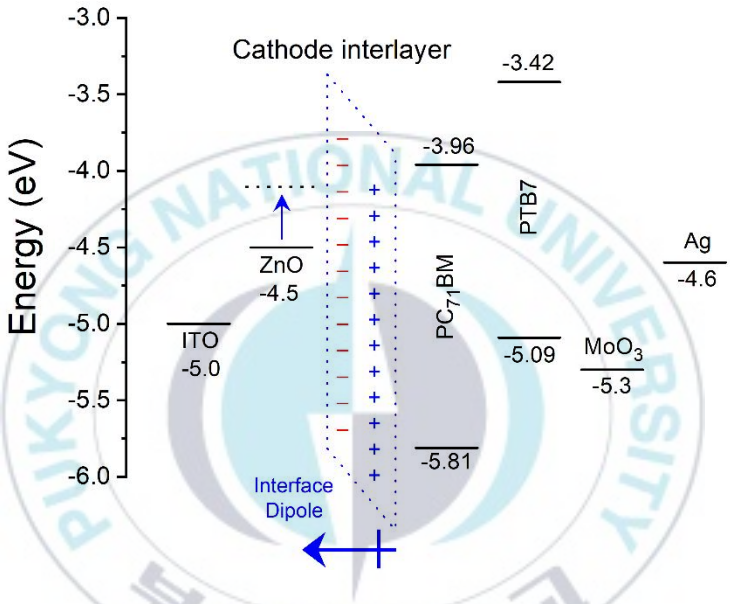

Figure Ⅰ - 5 The reduction of energy barrier after induction of interfacial dipole moment.

Ⅰ-iii General Parameters of Solar Cells

Ⅰ-iii-1. Short-Circuit Current (J_{SC})

A Short-circuit current (J_{SC}) is the current when the voltage on solar cells is zero (when the solar cell is a short circuit) [31]. J_{sc} is caused by the generation and collection of photo-induced charge carriers. The photo-induced current and J_{sc} are identical for ideal solar cells with moderate loss mechanisms due to resistance. Thus, J_{sc} is the maximum current that can be drawn from the solar cell. J_{sc} depends on various factors. First, it depends on the area of solar cells. Short-circuit current density [J_{sc}: mA/cm^2] is commonly used instead of short circuit current to eliminate dependence on the solar cell area [32]. Moreover, J_{sc} depends on the number of photons (output of incident light sources) and the incident light spectrum.

Ⅰ-iii-2. Open Circuit Voltage (V_{OC})

Open-circuit voltage (V_{oc}) is the maximum voltage that can be obtained from solar cells, which occurs when the current is zero (when the circuit is opened) [33]. V_{oc} corresponds to the amount of forward bias due to the bias on the solar cell junction with the photo-induced current. Furthermore, V_{oc} is a voltage at both ends of a solar cell when exposed to light without connection to the solar cell.

Ⅰ-iii-3. Fill Factor (FF)

Short-circuit current and open-circuit voltage are the maximum current and voltage of the solar cell, respectively. However, the power of solar cells is zero under these operating conditions. The fill factor (FF) is a factor that determines the maximum power of a solar cell with V_{oc} and J_{sc}. FF is the ratio of the maximum power of a solar cell to the product of V_{oc} and J_{sc} [34]. When the voltage and current giving the maximum power are V_{max} and J_{max}, respectively, the fill factor is defined as follows:

$$FF = \frac{J_{max} \times V_{max}}{J_{sc} \times V_{oc}} \qquad \textbf{(Equation Ⅰ - 1)}$$

The fill factor is a percentage of the maximum power obtained for the theoretically available power.

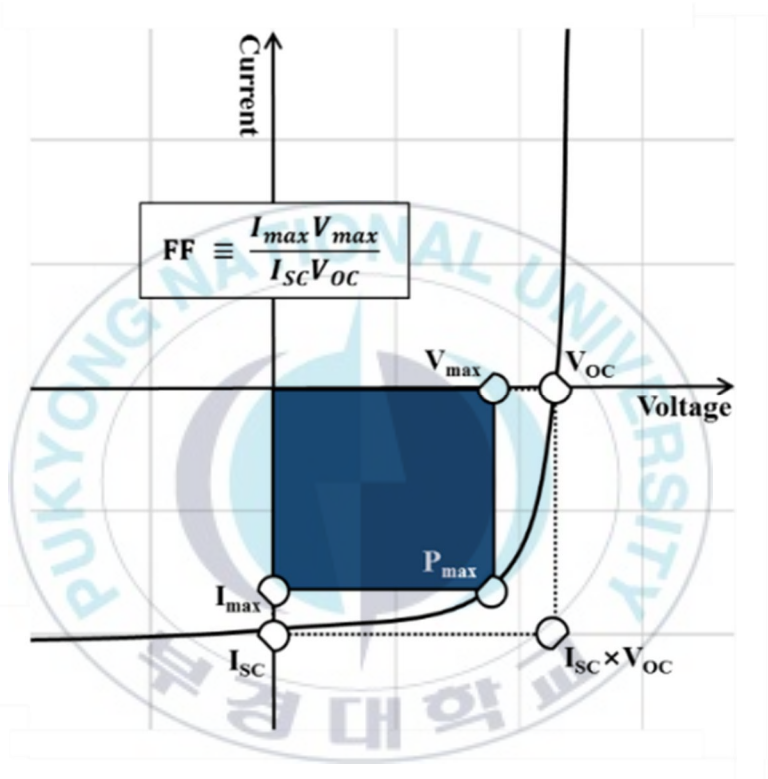

Figure Ⅰ - 6 The typical current-voltage (*I-V*) curve of solar cells.

Ⅰ-iii-4. Power Conversion Efficiency (PCE)

Power conversion efficiency (PCE) is the most efficient factor in comparing the performance of solar cells with other solar cells. The PCE is defined as the ratio of the maximum output power (P_{max}) from the solar cell to the input power (P_{in}) from the sunlight [35]. The P_{max} is defined as the product of J_{max} and V_{max}. According to the equation about FF above, the product of J_{max} and V_{max} can be represented by the multiplication of FF, J_{sc} and V_{oc}. Thus, PCE is defined as the following equation [36].

$$\eta = \frac{P_{max}}{P_{in}} = \frac{J_{max} \times V_{max}}{P_{in}} = \frac{FF \times J_{sc} \times V_{oc}}{P_{in}} \quad \textbf{(Equation Ⅰ - 2)}$$

Meanwhile, PCE depends on the spectrum and intensity of incident solar energy and solar cell temperature. Therefore, the conditions for measuring the efficiency of solar cells in order to compare the performance between solar cells should be carefully controlled. General solar cells are measured under the conditions of AM 1.5 and at temperatures of 25 °C [37].

Chapter Ⅱ

Simple Small Molecular Electrolytes as the Interlayer for Inverted Polymer Solar Cells

Ⅱ-ⅰ Introduction

Polymer solar cells (PSCs) as the photovoltaic device have great potential due to their low-cost fabrication process, lightweight and mechanical flexibility. Inverted PSCs (iPSCs) were introduced with long term stability since applied without acidic material, PEDOT:PSS, in conventional PSCs. To enhance the power conversion efficiencies (PCEs) of iPSCs, electron transport layers (ETLs) should become Ohmic contact between the electrode and active layer. Zinc Oxide (ZnO) is commonly used as the ETL in iPSCs, which has low work function and collects electrons with high mobility [38]. However, ZnO has indicated several disadvantages such as incompatibility between inorganic ZnO and organic materials for the active layer and high calcination temperature (up to 200 °C) [39]. To solve these problems, cathode interlayers (CIL) have been developed to modify the cathode interface. Conjugated polymers, non-conjugated polymers, organic small molecules, water/alcohol soluble conjugated polymers and biomaterials such as PFN [40], PEIE [41], $PNSO_3Na$ [42], PNDIT-F_3N-Br [43] and DNA [44] were used as the CIL. IPSCs with those materials showed the outperformed photovoltaic properties. On the other hand, polymers have disadvantages for synthesis such as batch to batch variation and complicated synthesis method [45]. Herein, simple small molecule electrolytes were designed to tune the cathode interface property, which have different length of alkyl chains to observe the influence of hydrophobicity. N^1,N^4-bis(2-hydroxyethyl)-N^1,N^1,N^4,N^4-tetramethylbutane-1,4-diaminium dibromide (**C4-OH**) and N^1,N^6-bis(2-hydroxyethyl)-N^1,N^1,N^6,N^6-tetramethylhexane-1,6-diaminium dibromide (**C6-OH**) (shown in **Figure Ⅱ-1**) were synthesized and fabricated with the device architecture of [ITO/ZnO/CIL/active layer/MoO_3/Ag] (shown in **Figure Ⅱ-2**).

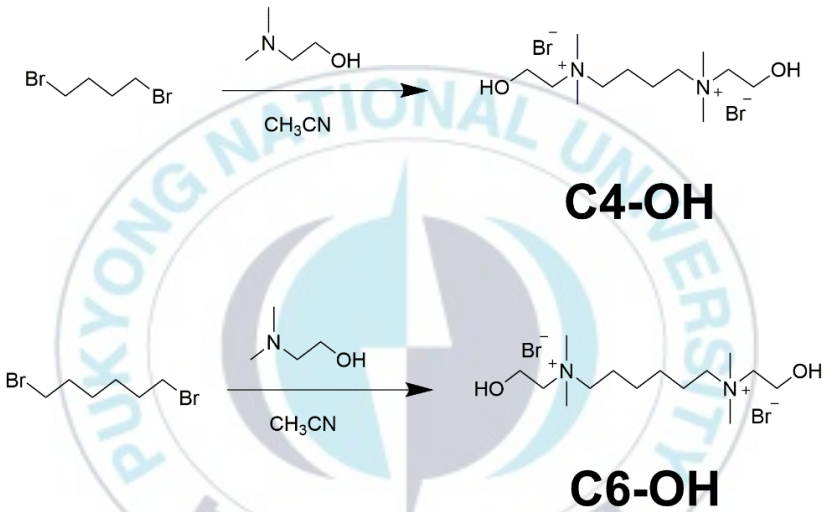

Figure Ⅱ-2 Chemical structures and synthesis procedure of **C4-OH** and **C6-OH**.

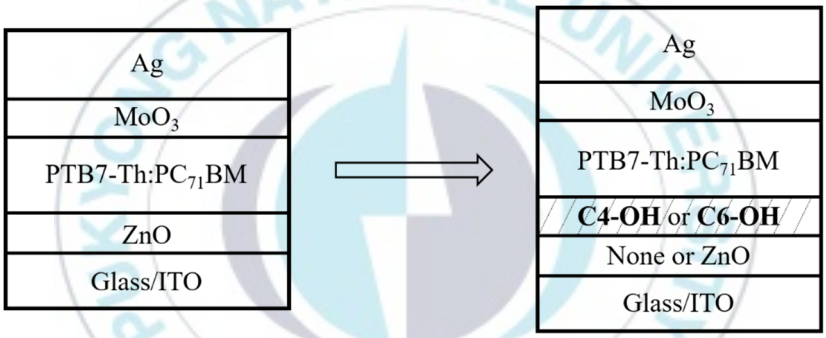

Figure Ⅱ-2 Device architecture of iPSCs based on **C4-OH** and **C6-OH.**

C4-OH and **C6-OH** consist of quaternary ammonium bromide and hydroxyl groups (─OH) to form a favorable interfacial dipole between the ZnO layer and the active layer.

Furthermore, the magnitude of the interfacial dipole moment will be increased by polar hydroxyl groups at the end of each material. A Schottky barrier at the cathode interface will be reduced owing to favorable interface dipole. PTB7-Th (Poly([2,6′-4,8-di(5-ethylhexylthienyl)benzo[1,2-b;3,3-b]dithiophene]{3-fluoro-2[(2-ethylhexyl)carbonyl]thieno[3,4-b]thiophenediyl}) and $PC_{71}BM$ ([6,6]-phenyl C71 butyric acid methyl ester) were used as the active layer of bulk-heterojunction (BHJ) PSCs (shown in **FigureⅡ-3**).

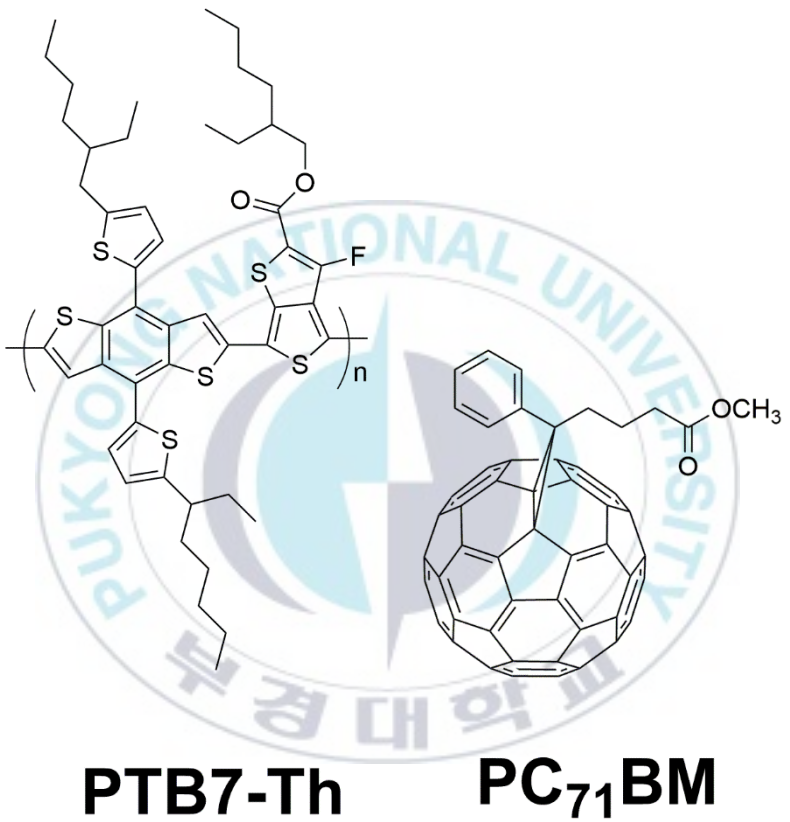

Figure Ⅱ-3 Chemical structures of PTB7-Th and $PC_{71}BM$ as the active layer.

As shown in **Table Ⅱ-1**, the PCEs of the devices with ZnO/**C4-OH** and ZnO/**C6-OH** were improved from 8.74 % (pristine ZnO) to 9.35 % (short circuit current density (J_{sc}) = 17.96 mA/cm^2, open-circuit voltage (V_{oc}) = 0.81 V, FF = 64.7 %) and 9.21 % (J_{sc} = 17.84 mA/cm^2, V_{oc} = 0.80 V, FF = 65.0 %), respectively. To fabricate the device without calcination process for ZnO layer, ZnO-free [ITO/CIL/active layer/MoO_3/Ag] devices were also applied. The PCEs of the devices were achieved up to the device based on pristine ZnO with device architecture of (shown in **Figure Ⅱ-2**).

Ⅱ-ii Experiment

Ⅱ-ii-1. Materials

All chemicals were purchased from Alfa Aesar or Sigma-Aldrich and used as received unless otherwise described. PTB7-Th (Poly([2,6′-4,8-di(5 ethylhexylthienyl) benzo[1,2-b;3,3-b]dithiophene]{3-fluoro-2[(2-ethylhexyl)carbonyl]thieno[3,4-b]thiophenediyl}) and $PC_{71}BM$ ([6,6]-phenyl C71 butyric acid methyl ester) were purchased from Derthon Co.

Ⅱ-ii-2. Synthesis

N^1,N^4-bis(2-hydroxyethyl)-N^1,N^1,N^4,N^4-tetramethylbutane-1,4-diaminium dibromide (C4-OH).

A mixture of 1,4-dibromobutane (0.864 g, 4.00 mmol) and 2-(dimethylamino)ethanol (0.749 g, 8.4 mmol) in acetonitrile was stirred at 70 °C for 12 hours. After cooling down to room temperature, white precipitates (**C4-OH**) were filtered and washed with a copious amount of acetonitrile and diethyl ether. ^{1}H NMR (400 MHz, CD_3OD ppm) δ 4.03~3.98 (m, 4H), 3.57~3.49 (m, 8H), 3.21~3.18 (s, 12H), 1.92~1.85 (m, 4H), 1.37~1.26 (t, 2H).

N^1,N^6-bis(2-hydroxyethyl)-N^1,N^1,N^6,N^6-tetramethylhexane-1,6-diaminium dibromide (C6-OH).

A mixture of 1,6-dibromohexane (0.976 g, 4.00 mmol) and 2-(dimethylamino)ethanol (0.749 g, 8.4 mmol) in acetonitrile was stirred at 70 °C for 12 hours. After cooling down to room temperature, white precipitates (**C6-OH**) were filtered and washed with a copious amount of acetonitrile and diethyl ether. ^{1}H NMR (600 MHz, CD_3OD, ppm) δ 4.04~4.01 (m, 4H), 3.54~3.51 (t, 4H), 3.49~3.45 (t, 4H), 3.21~3.20 (s, 12H), 1.92~1.86 (m, 4H), 1.56~1.47 (m, 6H), 1.39~1.31 (t, 2H).

Ⅱ-ii-3. Measurement

^{1}H NMR spectra were recorded on a JEOL JNM ECP-600 (or 400) spectrometer. Kelvin probe microscopy (KPM) measurements (KP technology Ltd. Model KP020) were performed to measure the work function of ZnO/**C4-OH**, ZnO/**C6-OH**, ITO/**C4-OH**, and ITO/**C6-OH**. The work function of the samples was estimated by measuring the contact potential difference between the sample and the KPM tip. The KPM tip was calibrated against a standard reference gold surface, with a work function of 5.1 eV. The thickness of the ZnO and the active layer was measured using an Alpha-Step IQ surface profiler (KLA-Tencor Co.). The current density-voltage measurements were performed under simulated light (AM 1.5G, 1.0 sun condition/100 mW/cm^{2}) from a 150 W Xe lamp, using a KEITHLEY Model 2400 source-measure unit. A calibrated Si reference cell with a KG5 filter certified by the National Institute of Advanced Industrial Science and Technology was used to confirm the 1.0 sun condition.

Ⅱ-ⅱ-4. Fabrication of PSCs

In order to fabricate the iPSCs with the device architecture of [ITO/ZnO (25 nm) or ZnO-free/CIL (~ 5 nm)/PTB7-Th:$PC_{71}BM$ (70 nm)/MoO_3 (3 nm)/Ag (100 nm)], a ZnO layer was deposited on the ITO substrate. ZnO solution was prepared by sol-gel process, which contained zinc acetate dihydrate (0.1 g) and 0.025 mL of ethanolamine in 1 mL of methoxyethanol and stirred for 12 hours at 60 °C and then cured at 200 °C for 10 min in air atmosphere. The thin film of each interlayer was spin-coated by using 1 mg/mL at 5000 rpm for 60 s. The active layer was spin-cast from a mixture of PTB7-Th and $PC_{71}BM$ (obtained by dissolving 10 mg of PTB7-Th and 15 mg of $PC_{71}BM$ in 1 mL of chlorobenzene with 3% (v/v) 1,8-diiodooctane (DIO)) at 1800 rpm for 120 s in N_2. The active solution was filtered through a 0.45 μm membrane filter before spin coating. Successive layers of MoO_3 and Ag were thermally evaporated through a shadow mask, with a device area of 0.09 cm^2 at 2 x 10^{-6} Torr.

Ⅱ-iii Results and discussion

IPSCs with the device architecture of ITO/ZnO or ZnO-free/**C4-OH** or **C6-OH** layer/active layer/MoO_3/Ag were fabricated to investigate the effect of CIL on the photovoltaic performances. Current density-voltage (*I-V*) curves of iPSCs with **C4-OH** and **C6-OH** under illumination and dark conditions are shown in **Figure Ⅱ-4** and **Figure Ⅱ-5**.

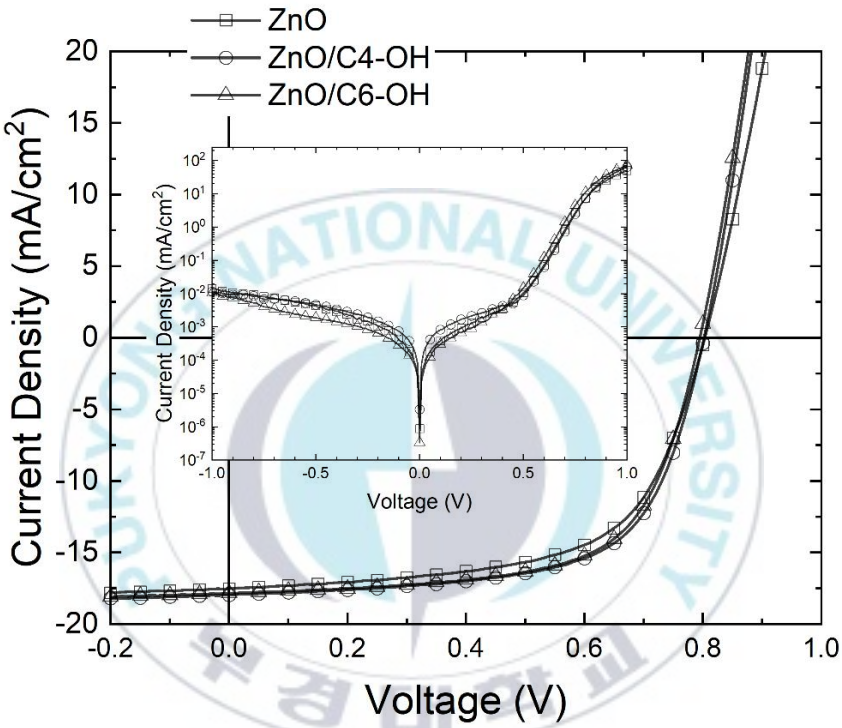

Figure Ⅱ-4 *I-V* curves based on the device architecture of [ITO/ZnO/CIL/active layer/MoO_3/Ag].

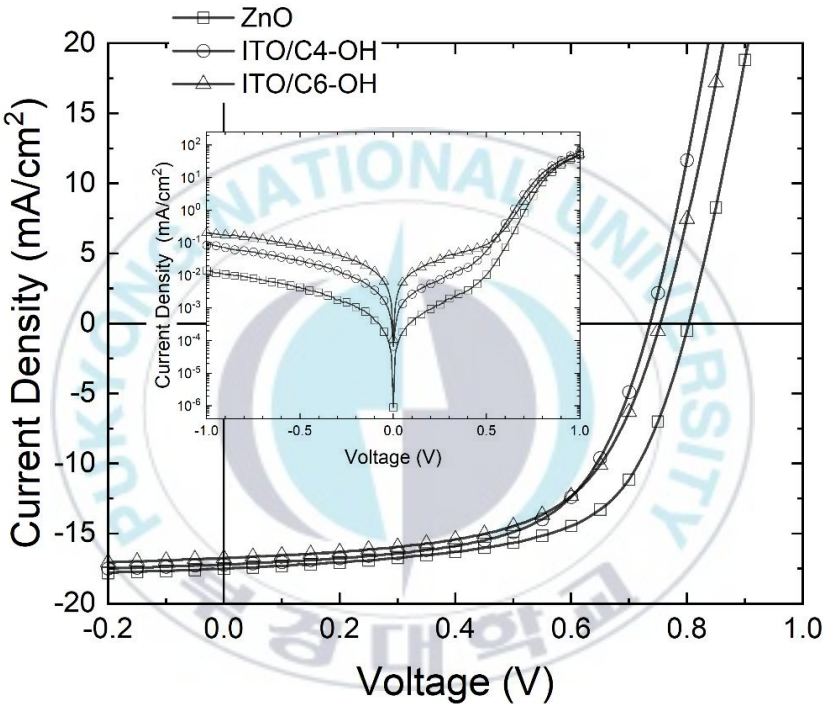

Figure Ⅱ-5 *I-V* curves based on the device architecture of [ITO/CIL/active layer/MoO_3/Ag].

The photovoltaic performances are summarized in **Table Ⅱ-1**. As shown in **Table Ⅱ-1**, improved J_{sc} and FF are the main contributions to enhancing the PCE. The J_{sc} of the device based on ZnO/**C4-OH** were increased from 17.52 mA/cm^2 (pristine ZnO) to 17.96 mA/cm^2 and FF were improved from 62.2 % (pristine ZnO) to 64.7 %. The J_{sc} and FF of the device based on ZnO/**C6-OH** were also increased up to 17.84 mA/cm^2 and 65.0 %, respectively. The V_{oc} of the device based on new CILs was same with that of the device without interlayer. As a result, the PCEs of the device with ZnO/**C4-OH** or **C6-OH** were improved from 8.74 % (J_{sc} = 17.52 mA/cm^2, V_{oc} = 0.80 V, FF = 62.2 %) to 9.35 % (J_{sc} = 17.96 mA/cm^2, V_{oc} = 0.81 V, FF = 64.7 %) and 9.21 % (J_{sc} = 17.84 mA/cm^2, V_{oc} = 0.80 V, FF = 65.0 %), respectively. The PCEs of the devices with ITO/**C4-OH** and ITO/**C6-OH** reached up to 7.70 % (J_{sc} = 7.23 mA/cm^2, V_{oc} = 0.74 V, FF = 60.8 %) and 7.55 % (J_{sc} = 16.77 mA/cm^2, V_{oc} = 0.76 V, FF = 59.6 %), respectively, which are slightly lower than that of the device based on pristine ZnO. Regardless of the low PCEs, **C4-OH** and **C6-OH** can be used as potential CIL to avoid the calcination with a high-temperature process. Kelvin probe microscopy (KPM) measurements were performed to investigate the effect of **C4-OH** and **C6-OH** on the work function (WF) (shown in **Figure Ⅱ-6 and Figure Ⅱ-7**), which indicate the relationship between the improvement of J_{sc} and the reduction of Schottky barrier. The WFs of ZnO/**C4-OH** or **C6-OH** were decreased from -4.50 eV (pristine ZnO) to -4.27 and -4.37 eV, respectively. Devices with ITO/**C4-OH** or **C6-OH** showed a lower WF (-4.58 eV and -4.62 eV, respectively) than the ITO (-5.0 eV). The PCEs were similar although **C4-OH** and **C6-OH** have different length of the alkyl chain. This is presumably owing to a little difference of alkyl length. The series resistance (R_s) followed the tendency of the photovoltaic performances, which are shown in **Table Ⅱ-1**. Calculated J_{sc} from incident photon-to-current efficiency (IPCE) curves (shown in **Figure Ⅱ-8**) are well matched with the J_{sc} of the devices.

Table Ⅱ-1 Photovoltaic parameters of iPSCs based on **C4-OH** and **C6-OH** with PTB7-Th:$PC_{71}BM$ as the active layer showing the best PCE. The averages are in parentheses.

ETL	J_{SC} (mA/cm^2)	V_{OC} (V)	FF (%)	PCE (%)	R_S (Ω·cm^2)
ZnO	17.52 (17.47)	0.80 (0.80)	62.2 (62.2)	8.74 (8.71)	3.1
ZnO/**C4-OH**	17.96 (17.92)	0.81 (0.80)	64.7 (64.1)	9.35 (9.20)	2.0
ZnO/**C6-OH**	17.84 (17.82)	0.80 (0.79)	65.0 (64.6)	9.21 (9.11)	2.1
ITO/**C4-OH**	17.23 (17.22)	0.74 (0.74)	60.8 (59.7)	7.70 (7.58)	2.7
ITO/**C6-OH**	16.77 (16.72)	0.76 (0.76)	59.6 (59.2)	7.55 (7.48)	2.8

[a] series resistance is calculated from the device showing the best PCE.

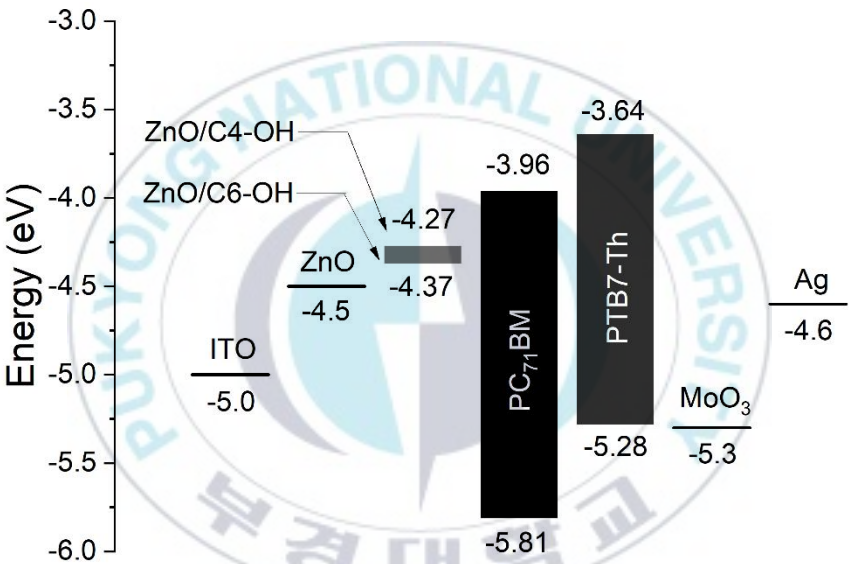

Figure Ⅱ-6 The work function of **C4-OH** and **C6-OH** layers with ZnO layer.

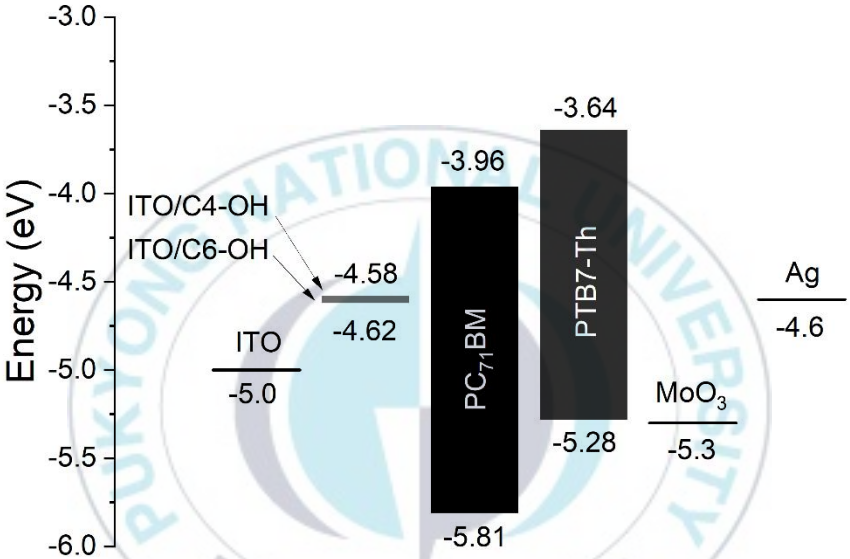

Figure Ⅱ-7 The work function of **C4-OH** and **C6-OH** layers with only ITO.

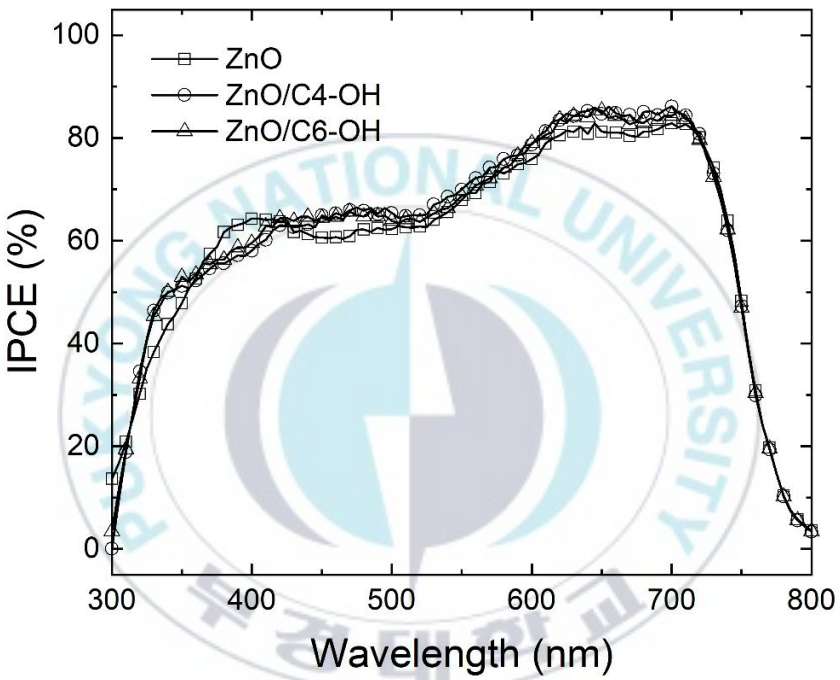

Figure Ⅱ-8 IPCE curves of the devices based on ZnO or ZnO/CILs.

Ⅱ-ⅳ Conclusion

We have successfully synthesized non-conjugated small molecule electrolytes (**C4-OH** and **C6-OH**) as the cathode interlayer. The influence of these materials on the photovoltaic properties in iPSCs was demonstrated. The reduction of the Schottky barrier was caused by the generation of the dipole at the cathode interface, which was proved through the KPM measurement. As a result, the iPSCs based on **C4-OH** and **C6-OH** showed outstanding photovoltaic performances.

Chapter Ⅲ

Small Molecular Electrolyte Hybridized ZnO for Polymer Solar Cells without Thickness Limitation

Ⅲ-ⅰ Introduction

In the previous work, inverted polymer solar cells (iPSCs) based on new small molecular electrolytes (C4-OH and C6-OH) were fabricated, which showed improved power conversion efficiencies (PCEs). An important issue in the previous was tuning the energy offset at the cathode interface to modify the electron collection capability. However, these iPSCs have the disadvantage that it is difficult to apply to real industrial processes even though it can show better PCEs by introducing interlayers in iPSCs. This disadvantage is caused by the inherent electrical insulating properties of interlayer materials, which leads to maintaining a thin film of less than 5 nm when the interlayer is introduced in iPSCs with increased PCEs [46]. Thus, the hybridized ZnO layer as an electron transport layer (ETL) was introduced as a new method of fabricating the device to overcome this thickness dependence problem [47]. This hybridization is the introduction of interlayer materials into the ZnO layer when making ZnO solutions. It is unnecessary to maintain a thin film of less than 5 nm, which can maintain a thickness of about 25 nm, the same as the ZnO layer.

We designed and synthesized N^1,N^6-bis(2-hydroxyethyl)-N^1,N^1,N^6,N^6-tetramethylhexane-1,6-diaminium bis(4-methylbenzenesulfonate) (**C6-E-OTs**) (shown in **FigureⅢ-1**) to hybridized with ZnO for outstanding iPSCs. Furthermore, we also synthesized N^1,N^6-bis(2-hydroxyethyl)-N^1,N^1,N^6,N^6-tetramethylhexane-1,6-diaminium dibromide (**C6-E-Br**) to compare with **C6-E-OTs** in terms of anion size. The dipole moment of the ionic compounds is proportional to the distance between the two charges [48]. Therefore, the dipole moment of **C6-E-OTs** would be larger than that of **C6-E-Br**. A higher dipole moment of electrolyte would induce a higher electrical conductivity. Thus, we replaced the counter anion of the molecule from bromide (Br) to 4-methylbenzenesulfonate (OTs). In addition to this, the solubility of the electrolytes with OTs (**C6-E-OTs**) as the counter anion in polar protic solvent was observed to be much better than the compounds with Br (**C6-E-Br**).

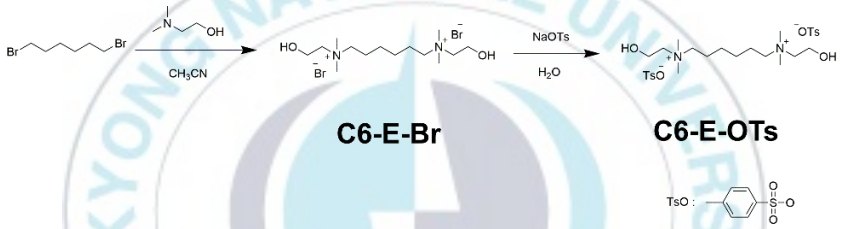

FigureⅢ-2 Chemical structures and synthesis procedure of **C6-E-Br** and **C6-E-OTs**.

As illustrated in **FigureⅢ-2**, iPSCs with **C6-E-OTs** hybridized ZnO layers as the ETLs were fabricated. In addition, iPSC with **C6-E-OTs** as the interlayer was also fabricated to compare with the hybridized ZnO layer. Hydroxyl (-OH) groups in **C6-E-OTs** chemically bonded to Zn atoms and thus transparent hybridized ZnO layer with **C6-E-OTs** was produced. The device based on bulk-heterojunction (BHJ) structures composed of PTB7 (poly({4,8-bis[(2-ethylhexyl)oxy]benzo[1,2-b:4,5-b′]dithiophene-2,6-diyl} {3-fluoro-2-[(2-ethylhexyl)carbonyl]thieno[3,4-b]thiophenediyl})) and $PC_{71}BM$ ([6,6]-phenyl C71 butyric acid methyl ester) as the active layer (shown in **FigureⅢ-3)** enhances the PCE from 7.6 % (short circuit current (J_{sc}) = 16.0 mA/cm^2, open-circuit voltage (V_{oc}) = 0.72 V, fill factor (FF) = 65.6 %) based on ZnO to 8.8 % (J_{sc} = 17.6 mA/cm^2, V_{oc} = 0.72 V, FF = 67.6 %) by introducing the **C6-E-OTs** hybridized ZnO layer. Moreover, the PCE of the devices based on **C6-E-OTs** is superior to the device based on **C6-E-Br** (shown in **TableⅢ-1**) due to that a larger counter anion induces a larger interface dipole. The main contribution for the PCE enhancement resulted from the improvement of the J_{sc} owing to the reduction of energy offset at the cathode interface.

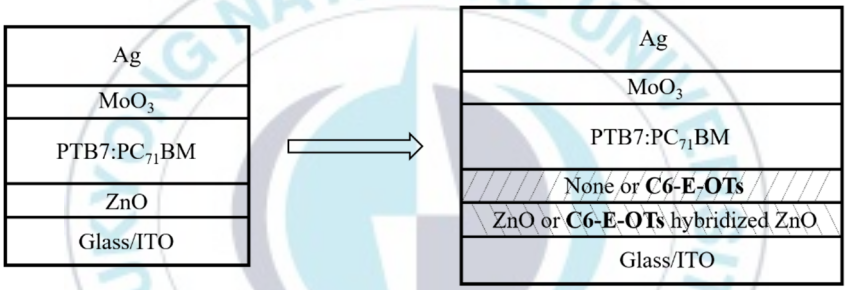

FigureⅢ-2 Device architecture of iPSCs based on **C6-E-OTs**.

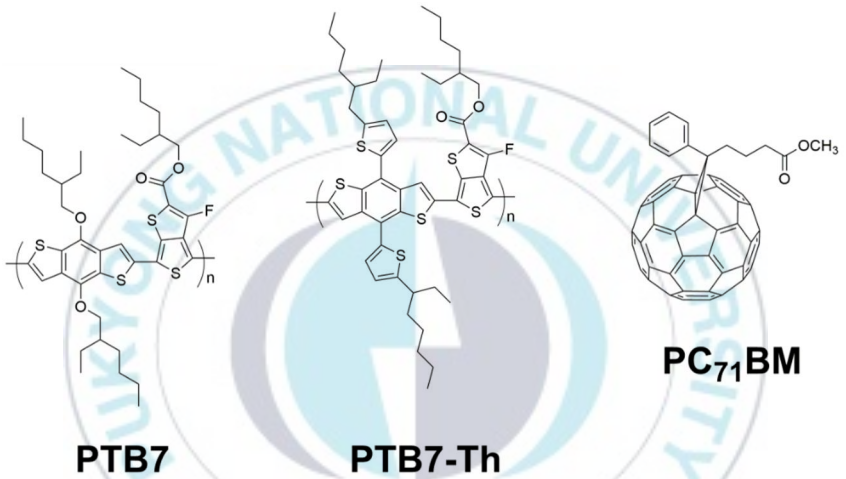

FigureⅢ-3 Chemical structures of PTB7, PTB7-Th and $PC_{71}BM$ as the active layer.

Ⅲ-ⅱ Experiment

Ⅲ-ⅱ-1. Materials

All chemicals were purchased from Alfa Aesar or Sigma-Aldrich and used as received unless otherwise described. PTB7 (Poly({4,8-bis[(2-ethylhexyl)oxy]benzo[1,2-*b*:4,5-b′]dithiophene-2,6-diyl}{3-fluoro-2-[(2-ethylhexyl)carbonyl]thieno[3,4-b]thiophenediyl})), Poly([2,6′-4,8-di(5-ethylhexylthienyl)benzo[1,2-b;3,3-b]dithiophene]{3-fluoro-2[(2ethylhexyl)carbonyl]thieno[3,4-b]thiophenediyl}) (PTB7-Th) and $PC_{71}BM$ ([6,6]-phenyl C71 butyric acid methyl ester) (Cat No. nano-cPCBM-SF) were purchased from 1-material Co., Derthon optoelectronic materials science technology Co. LTD, and nano-C, Inc., respectively.

Ⅲ-ⅱ-2. Synthesis

N^1,N^6-bis(2-hydroxyethyl)-N^1,N^1,N^6,N^6-tetramethylhexane-1,6-diaminium bis(4-methylbenzenesulfonate) (C6-E-OTs).

A mixture of 1,6-dibromohexane (0.976 g, 4.00 mmol) and 2-(dimethylamino)ethanol (0.749 g, 8.4 mmol) in acetonitrile was stirred at 70 °C for 12 hours. After cooling down to room temperature, white precipitates (**C6-E-Br**) were filtered and washed with a copious amount of acetonitrile and diethyl ether. Ion exchange reaction proceeded without purification. A solution of sodium 4-methylbenzenesulfonate (1.165 g, 6.00 mmol) in 10.0 mL deionized water was added dropwise in a solution of **C6-E-Br** (0.844 g, 2.00 mmol) in 10.0 mL of deionized water. After finish to the addition of a solution of sodium 4-methylbenzenesulfonate (1.165 g, 6.00 mmol), the mixture was stirred for 12 hours. The white precipitates (**C6-E-OTs**) were filtered and washed with a copious amount of deionized water. ^{1}H NMR (600 MHz, CD_3OD, ppm) δ 7.69~7.66 (d, 2H), 7.25~7.21 (d, 2H), 3.97~3.93 (t, 2H), 3.45~3.42 (t, 2H), 3.39~3.36 (t, 2H), 3.12 (s, 6H), 2.36 (s, 3H), 1.83~1.78 (m, 2H), 1.45~1.41 (m, 2H). ^{13}C NMR (150 MHz, DMSO-D_6, ppm) δ 145.63, 137.72, 128.11, 125.48, 64.60, 63.92, 54.97, 50.79, 25.22, 21.53, 20.79. Anal. Calcd. For $C_{28}H_{48}N_2O_8S_2$: C, 55.60; H, 8.00; N, 4.63; S, 10.60. Found: C, 55.4; H, 7.89; N, 4.57; S, 10.34.

Ⅲ-ⅱ-3. Measurement

^{1}H and ^{13}C NMR spectra were recorded on a JEOL JNM ECP-600 spectrometer. The thickness of the ZnO and the active layer was measured using an Alpha-Step IQ surface profiler (KLA-Tencor Co.). Thermogravimetric analysis (TGA) of the polymers was carried out under the air atmosphere at a heating rate of 10 °C/min with a thermogravimetric analyzer (Thermal Analysis 2050, TA Instruments). The crystallinity of the samples was tested by X-ray diffraction (XRD), using a Bruker D8 Focus X-ray diffractometer operating at 30 kV and 20 mA with a Cu target (λ = 1.54 A) at a scanning rate of 0.02 °/s (2 ~ 80 °). Static water contact angle images were captured after placing a 3 μL drop on the substrate and were performed using a contact angle measurement system (KRUSS, Model DSA 100). Atomic force microscopy (AFM) images were captured using a Bruker (NanoScope V) AFM in the tapping mode. The water contact angles of the substrates were measured using KRUSS Model DSA 100. Kelvin probe microscopy (KPM) measurements (KP technology Ltd. Model KP020) were performed to measure the work function of ZnO layers with and without **C6-E-OTs**, and the work function of the samples was estimated by measuring the contact potential difference between the sample and the KPM tip. The KPM tip was calibrated against a standard reference gold surface, with a work function of 5.1 eV. The current density-voltage measurements were performed under simulated light (AM 1.5G, 1.0 sun condition/100 mW/cm^2) from a 150 W Xe lamp, using a KEITHLEY Model 2400 source-measure unit. A calibrated Si reference cell with a KG5 filter certified by the National Institute of Advanced Industrial Science and Technology was used to confirm the 1.0 sun condition.

Ⅲ-ⅱ-4. Fabrication of iPSCs

In order to fabricate the iPSCs with the device architecture [ITO/ZnO or **C6-E-OTs** hybridized ZnO (25 nm)/active layer (PTB7 or PTB7-Th:$PC_{71}BM$, 70 nm)/MoO_3 (3 nm)/Ag (100 nm)], a ZnO layer was deposited on an ITO substrate by the sol-gel process. Zinc acetate dihydrate (0.1 g) with 5, 10.0, 13.0 wt. % of **C6-E-OTs** and 0.025 mL of ethanolamine were dissolved in 1 mL of methoxyethanol and stirred for 12 hours at 60 °C. A thin film of ZnO or **C6-E-OTs** hybridized ZnO sol-gel precursor was spin-coated at 4000 rpm for 60 s then cured at 200 °C for 10 min. The active layer was spin-cast from a mixture of PTB7 (or PTB7-Th) and $PC_{71}BM$ (obtained by dissolving 10 mg of PTB7 (or PTB7-Th) and 15 mg of $PC_{71}BM$ in 1 mL of chlorobenzene with 3 % (v/v) 1,8-diiodooctane (DIO)) and rotated at 1800 rpm for 120 s. The active solution was filtered through a 0.45 μm membrane filter before spin coating. Successive layers of MoO_3 and Ag were thermally evaporated through a shadow mask, with a device area of 0.09 cm^2 at 2 x 10^{-6} Torr.

Ⅲ-ⅱ-5. Fabrication of electron-only devices

Electron-only devices with the architecture [ITO/ZnO or **C6-E-OTs** hybridized ZnO (55 nm)/Al (100 nm) and ITO/ZnO or **C6-E-OTs** hybridized ZnO (30 nm)/$PC_{71}BM$ (60 nm)/Al (100 nm)], have been fabricated to investigate the electron mobility of hybridized or pristine ZnO layer.

Ⅲ-iii Results and discussion

Ⅲ-iii-1. Characterization of C6-E-OTs Hybridized ZnO.

Thermogravimetric analysis (TGA) (**FigureⅢ-4**) of **C6-E-OTs** was carried out at a heating rate of 10 °C min^{-1} under the air. According to the TGA thermogram, **C6-E-OTs** was thermally stable up to 322 °C (the temperature of 5 % weight loss exhibited at 322 °C). We performed X-ray photoelectron spectroscopy (XPS) to analyze the existence of **C6-E-OTs** in the ZnO layer. As shown in **FigureⅢ-5**, peaks at the binding energies (BEs) of 398 and 166 eV correspond to N 1s and S 2p, respectively. These peaks did not appear in the survey spectrum of ZnO. Thus, the survey spectra confirmed the existence of **C6-E-OTs** in the ZnO layer. Peaks at BEs of 1044 and 1021 eV in the XPS spectrum in ZnO correspond to Zn $2p_{1/2}$ and $2p_{3/2}$, respectively. The BEs of corresponding peaks of **C6-E-OTs** in ZnO shifted toward a higher BE because the Zn atoms in the hybridized ZnO matrix were more electron-rich than those of the pristine ZnO matrix (**FigureⅢ-6**). In the X-ray diffraction (XRD) spectra (**FigureⅢ-7**) of **C6-E-OTs** hybridized ZnO, no discernible diffraction patterns are observed. This means that the addition of **C6-E-OTs** deteriorates the ordering of ZnO. The water contact angle and the atomic force microscopy (AFM) were performed to investigate the surface properties of the ZnO and **C6-E-OTs** hybridized ZnO layer. As shown in **FigureⅢ-8**, the water contact angle of the surface of **C6-E-OTs** hybridized ZnO was observed to be smaller than that of the ZnO surface without **C6-E-OTs** due to unreacted free –OH groups on the surface. AFM images of **C6-E-OTs** hybridized ZnO surface (**FigureⅢ-9**) were observed to be almost identical to that of ZnO with the surface roughness of 1.30–1.46 nm. The morphology of the surface did not seem to be affected by **C6-E-OTs** in the ZnO.

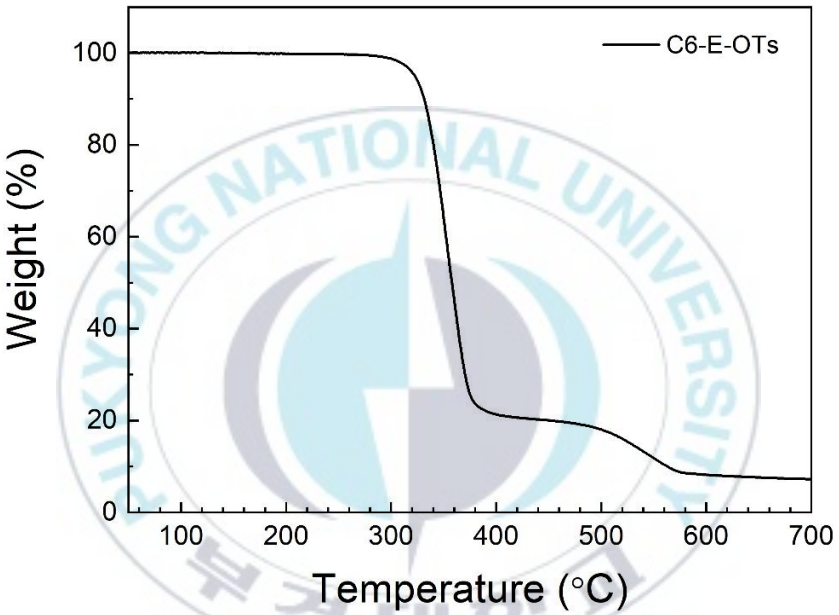

FigureⅢ-4 TGA thermograms of **C6-E-OTs**.

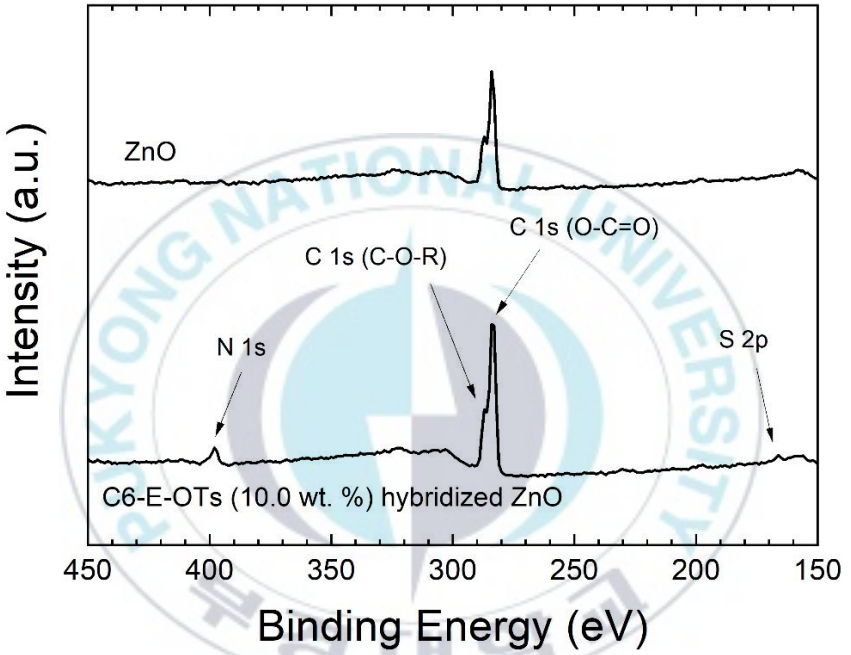

FigureⅢ-5 XPS survey spectra of ZnO and 10.0 wt. % of **C6-E-OTs** hybridized ZnO.

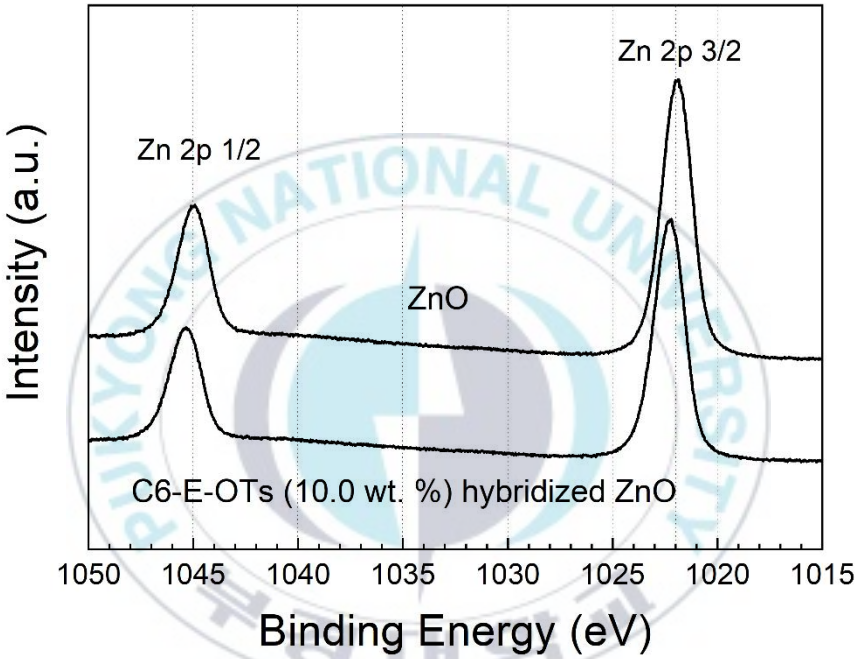

FigureⅢ-6 XPS Zn 2p spectra of ZnO and 10.0 wt. % of **C6-E-OTs** hybridized ZnO.

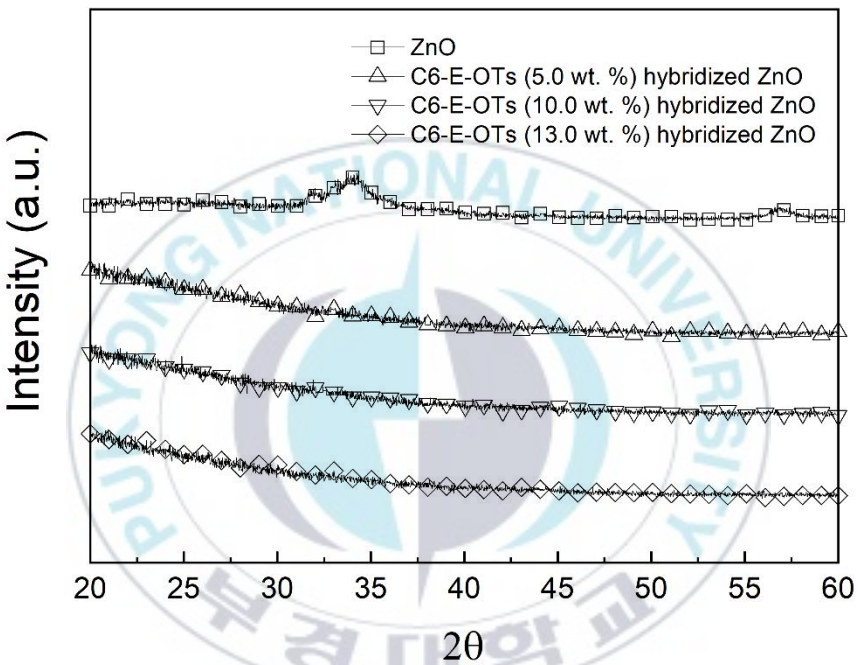

FigureⅢ-7 XRD patterns of ZnO and **C6-E-OTs** hybridized ZnO.

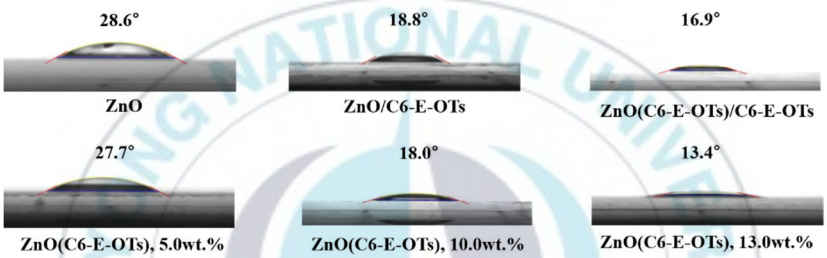

FigureⅢ-8 Static water contact angle of ZnO, thin layer (5 nm) of **C6-E-OTs** coated on ZnO, **C6-E-OTs** (5.0 wt. %) hybridized ZnO, **C6-E-OTs** (10.0 wt. %) hybridized ZnO, **C6-E-OTs** (13.0 wt. %) hybridized ZnO, and thin layer of **C6-E-OTs** (5 nm) coated on **C6-E-OTs** (10.0 wt. %) hybridized ZnO.

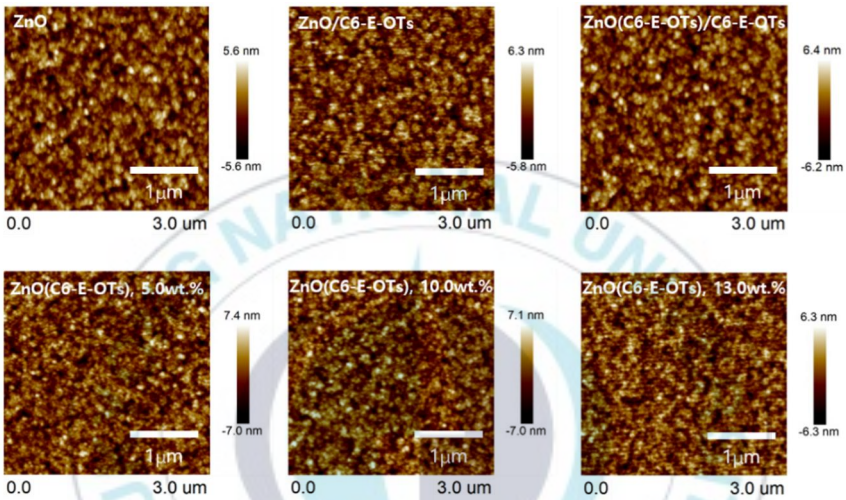

FigureⅢ-9 AFM images of ZnO, thin layer (5 nm) of **C6-E-OTs** coated on ZnO, **C6-E-OTs** (5.0 wt. %) hybridized ZnO, **C6-E-OTs** (10.0 wt. %) hybridized ZnO, **C6-E-OTs** (13.0 wt. %) hybridized ZnO, and thin layer of **C6-E-OTs** (5 nm) coated on **C6-E-OTs** (10.0 wt. %) hybridized ZnO.

Ⅲ-iii-2. Photovoltaic properties.

ZnO layer with or without **C6-E-OTs** as the electron transport layer in iPSCs with the architecture of [ITO/ZnO or **C6-E-OTs** hybridized ZnO/PTB7:$PC_{71}BM$/MoO_3/Ag (shown in **FigureⅢ-2**) were fabricated and tested to understand the effect of **C6-E-OTs** on the performance of the devices. The ZnO layer with different concentrations (5.0, 10.0, and 13.0 wt. %) of **C6-E-OTs** prepared by the typical sol-gel process. The transmittance spectra of ZnO with different concentrations of **C6-E-OTs** are displayed in **FigureⅢ-10**. **FigureⅢ-11** shows current density–voltage (*I-V*) curves of iPSCs with or without **C6-E-OTs** under illumination while the photovoltaic parameters have been summarized in **TableⅢ-2**. As shown in **FigureⅢ-11** and **TableⅢ-3**, the optimum concentration of **C6-E-OTs** in the ZnO layer with the best PCE was determined to be 10.0 wt. % while the PCE of the device based on ZnO without **C6-E-OTs** was limited to 7.4 % (J_{sc} = 16.0 mA/cm^2, V_{oc} = 0.72 V, FF = 65.6 %). Thus, significant improvements were observed in the devices based on ZnO with **C6-E-OTs**. The PCEs of the devices with 10.0 wt. % of **C6-E-OTs** hybridized ZnO layer and **C6-E-OTs** as the interlayer (~ 5 nm), exhibited 8.8 % (J_{sc} = 17.6 mA/cm^2, V_{oc} = 0.74 V, FF = 67.6 %) and 8.5 % (J_{sc} = 17.6 mA/cm^2, V_{oc} = 0.72 V, FF = 67.6 %), respectively. It should be noted that the main contribution to improving the PCE was the enhanced J_{sc}. We also fabricated and tested the device with 10.0 wt. % of **C6-E-OTs** hybridized ZnO and the thin layer of **C6-E-OTs** as the interlayer, simultaneously. The PCE of the device was 8.9 % (J_{sc} = 17.9 mA/cm^2, V_{oc} = 0.73 V, FF = 67.9 %), which provided for a 17.1 % enhancement compared with the device based on ZnO because of the synergy effect of hybridization and interlayer. Similar features were observed in the device with PTB7-Th as the donor polymer (see **TableⅢ-2**). The presence of **C6-E-OTs** hybridized ZnO and 5 nm of **C6-E-OTs** as the interlayer significantly improved the PCE from 8.0 % (J_{sc} = 15.6 mA/cm^2, V_{oc} = 0.80 V,

FF = 64. 2 %) to 9.4 % (J_{sc} = 17.9 mA/cm^2, V_{oc} = 0.81 V, FF = 65.0 %), and resulted in an enhancement of 17.5 %.

We performed the Kelvin probe microscopy (KPM) measurements, which is a well-known and powerful tool for investigating the effective work function at the ZnO interface, to investigate the effect of **C6-E-OTs** on the J_{sc} changes. A larger energy offset at the electrode interface interrupts the charge collection. Therefore, reducing energy offset at the electrode interface is an essential factor in achieving a high J_{sc}. As shown in **FigureⅢ-12**, the work function of ZnO with 10.0 wt. % **C6-E-OTs** hybridized ZnO and 5 nm thick **C6-E-OTs**, simultaneously, showed the highest work function (-4.08 eV) among **C6-E-OTs** treated ZnO layers. The work function of **C6-E-OTs** hybridized ZnO depends on the concentration of **C6-E-OTs**. However, the work function of hybridized ZnO does not show a linear relationship with the **C6-E-OTs** concentration. Note that the increase in the J_{sc} agreed well with the work function of **C6-E-OTs** hybridized or coated ZnO. However, the work function change did not show an agreement with the change in the V_{oc}. The series resistance (R_s) data and incident photon-to-current efficiency (IPCE) curves (**FigureⅢ-13**) of the devices showed good agreement with the performances of the devices. The series resistance of the devices with 5.0, 10.0 wt. % of **C6-E-OTs**, and 10.0 wt. % of **C6-E-OTs** hybridized ZnO layer and **C6-E-OTs** as the interlayer were 1.9, 2.1, and 2.8 Ω cm^2, which are smaller than those of the devices with 5.0 (3.2 Ω cm^2), 10.0 wt. % (2.7 Ω cm^2) of **C6-E-Br**, and 10.0 wt. % of **C6-E-Br** in ZnO layer and **C6-E-Br** (2.5 Ω cm^2) (see **TableⅢ-3**). The results support that a higher dipole moment of electrolyte would induce a higher electrical conductivity.

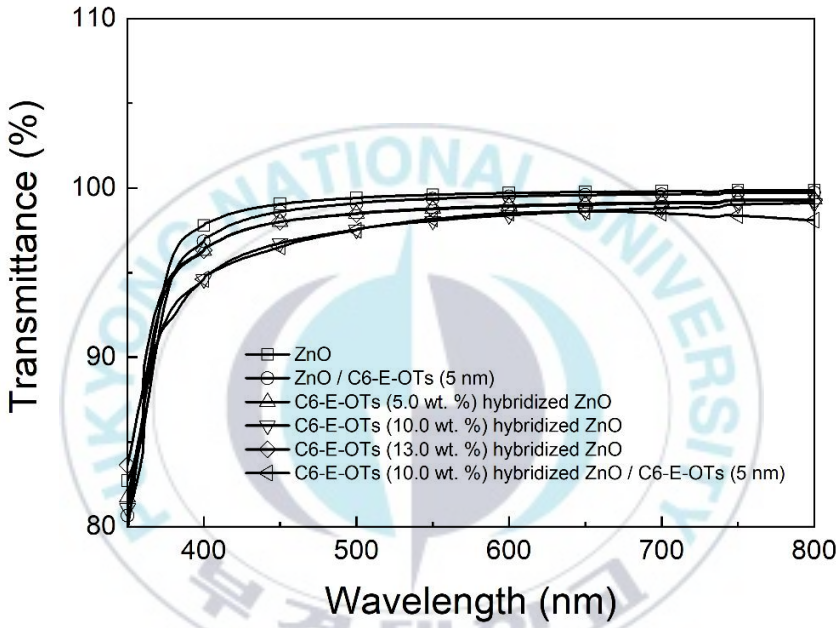

FigureⅢ-10 Transmittance spectra of the different concentration of **C6-E-OTs** in ZnO layer.

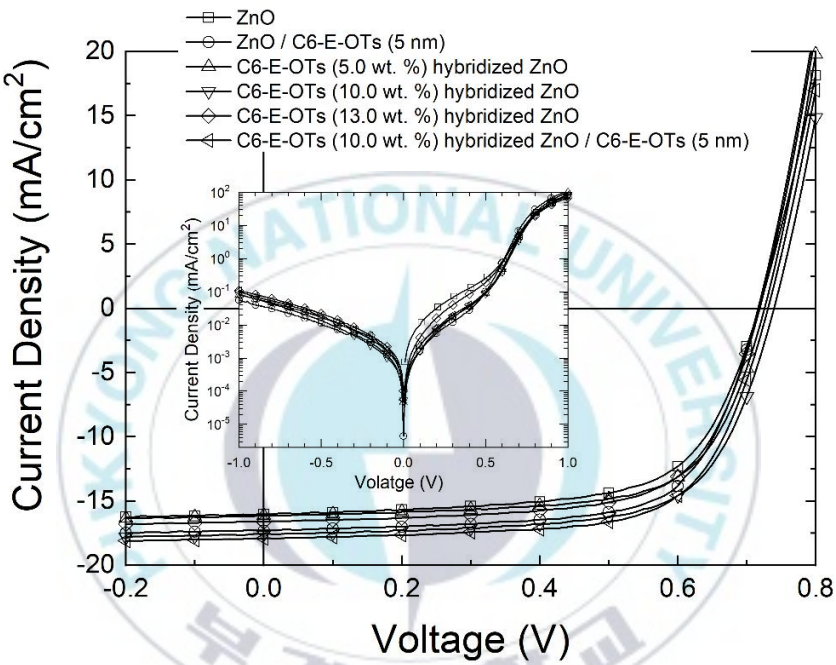

FigureⅢ-11 Current density–voltage curves of iPSCs under illumination (inset: in the dark condition).

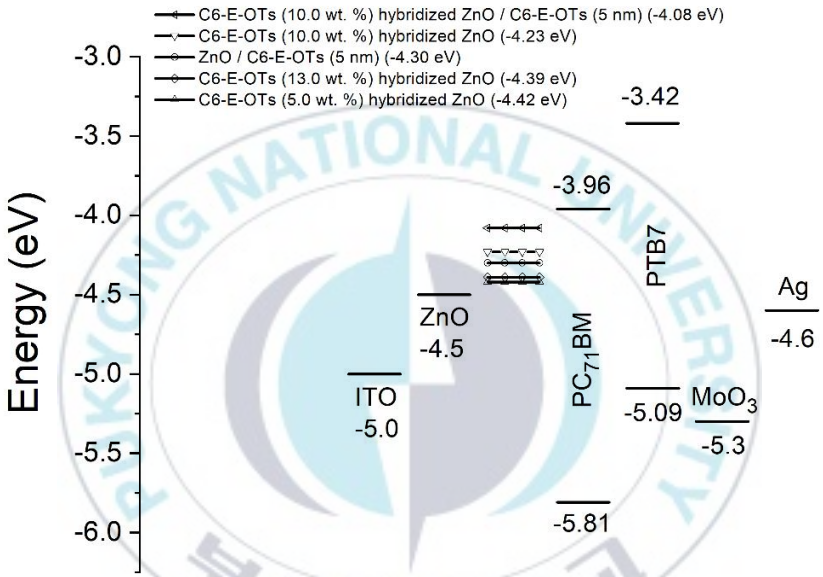

FigureⅢ-12 The work function of **C6-E-OTs** hybridized ZnO and thin layer of **C6-E-OTs** on ZnO.

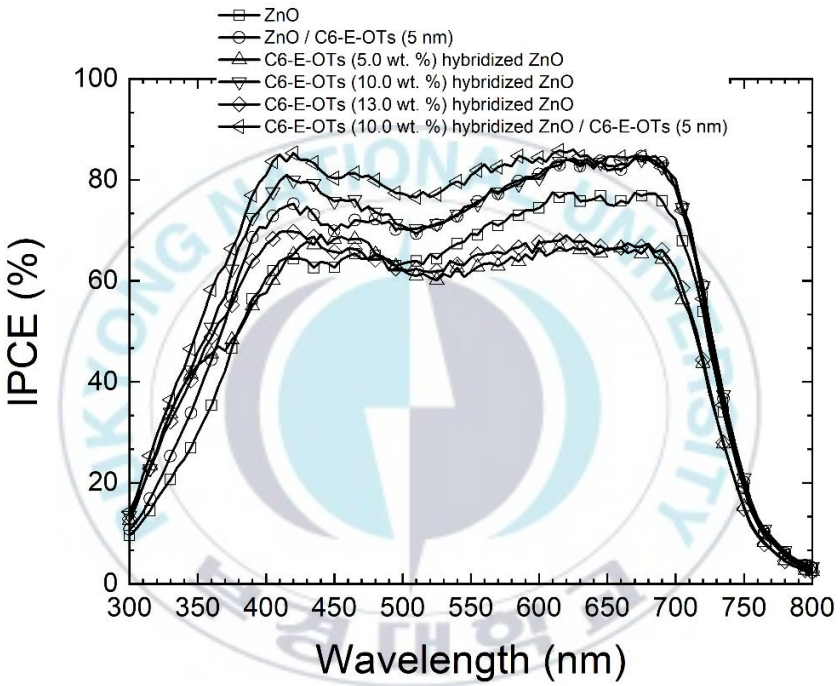

FigureⅢ-13 Incident photon-to-current efficiency (IPCE) curves of iPSCs.

To elucidate the electron transporting property of ZnO, we fabricated and tested the electron only devices with an architecture of [ITO/ZnO or **C6-E-OTs** hybridized ZnO (55 nm)/Al (100 nm). The electron mobilities of the devices **FigureⅢ-14**) were calculated by the space-charge limited current (SCLC) method. The electron mobilities of 5 nm thick **C6-E-OTs** as the interlayer on ZnO, 5.0 wt. % of **C6-E-OTs** hybridized ZnO, 10.0 wt. % of **C6-E-OTs** hybridized ZnO, 13.0 wt. % of **C6-E-OTs** hybridized ZnO, and 10.0 wt. % of **C6-E-OTs** hybridized ZnO and 5 nm thick **C6-E-OTs** as the interlayer were 1.24×10^{-3}, 1.16×10^{-3}, 1.33×10^{-3}, 1.04×10^{-3}, and 1.65×10^{-3} cm^2 V^{-1} s^{-1}, respectively, which are slightly higher than that of ZnO layer without **C6-E-OTs** (1.04×10^{-3} cm^2 V^{-1} s^{-1}). However, it is noted that the electron mobilities of the ZnO layer showed a good relationship with the J_{sc} data of the iPSCs. Interestingly, even though the diffraction patterns in XRD spectra significantly disappeared upon the addition of **C6-E-OTs**, the electron mobilities are slightly improved with the increasing amount of **C6-E-OTs** in ZnO.

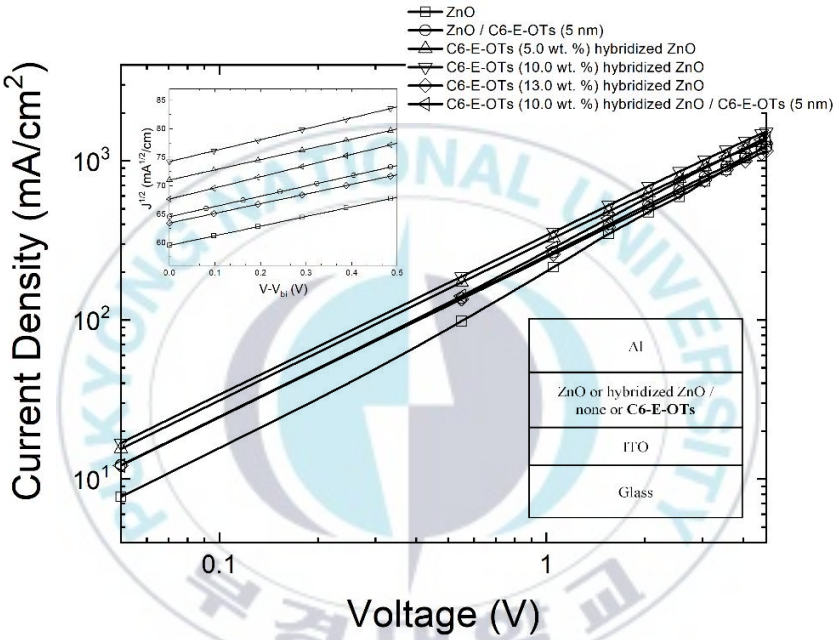

FigureⅢ-14 Current density as a function of voltage curves of electron-only device without $PC_{71}BM$ (V, applied voltage; V_{bi}, built-in voltage).

To further investigate the effect of **C6-E-OTs** on the properties of ZnO, we fabricated and tested electron-only devices composed of [ITO/ZnO or **C6-E-OTs** hybridized ZnO (30 nm)/$PC_{71}BM$ (60 nm)/Al (100 nm)] (**FigureⅢ-15**). From these devices, we can obtain information regarding the electron injection properties from the ZnO layer to the $PC_{71}BM$, which is known to be directly related to the electron collection properties of the ZnO layer. The electron mobilities of the devices based on ZnO/**C6-E-OTs** as the interlayer, 5.0 wt. % of **C6-E-OTs** hybridized ZnO, 10.0 wt. % of **C6-E-OTs** hybridized ZnO, 13.0 wt. % of **C6-E-OTs** hybridized ZnO, and 10.0 wt. % of **C6-E-OTs** hybridized ZnO and **C6-E-OTs** as the interlayer were 8.47×10^{-4}, 8.10×10^{-4}, 8.73×10^{-4}, 8.13×10^{-4}, and 9.13×10^{-4} cm^2 V^{-1} s^{-1}, respectively, which were slightly higher than that of ZnO layer without **C6-E-OTs** (8.07×10^{-4} cm^2 V^{-1} s^{-1}). The trend appeared to be almost same as the one obtained in the analysis of the electron mobility data of electron-only devices without $PC_{71}BM$. The turn-on voltages of the devices with ZnO, 5 nm of **C6-E-OTs** as the interlayer on ZnO, 5.0 wt. % of **C6-E-OTs** hybridized ZnO, 10.0 wt. % of **C6-E-OTs** hybridized ZnO, 13.0 wt. % of **C6-E-OTs** hybridized ZnO, and 10.0 wt. % of **C6-E-OTs** hybridized ZnO and 5 nm of **C6-E-OTs** as the interlayer were 1.40, 1.12, 1.19, 1.01, 1.18, and 0.99 V, respectively. Interestingly, the device based on 10.0 wt. % of **C6-E-OTs** hybridized ZnO and 5 nm of **C6-E-OTs** as the interlayer simultaneously exhibited the lowest turn-on voltage of 0.99 V among all the devices. Increased electron injection capability, in turn, led to an increase of the electron collection ability in the iPSCs. This has been well correlated to the energy offset at the cathode interface. The devices were kept in a glove box filled with N_2 gas without passivation. After 30 and 50 days, the PCE of the device based on pristine ZnO maintained 93 % and 87 % of its initial PCE. However, the PCE of the device based on 10.0 wt. % of **C6-E-OTs** hybridized ZnO with 5 nm thick **C6-E-OTs** interlayer maintained 95 % and 91 %, respectively, of its initial PCE under the same condition. The PCE of iPSC based on 10.0 wt. % of **C6-E-OTs** hybridized ZnO with 5 nm thick **C6-E-OTs**

interlayer showed better stability than others.

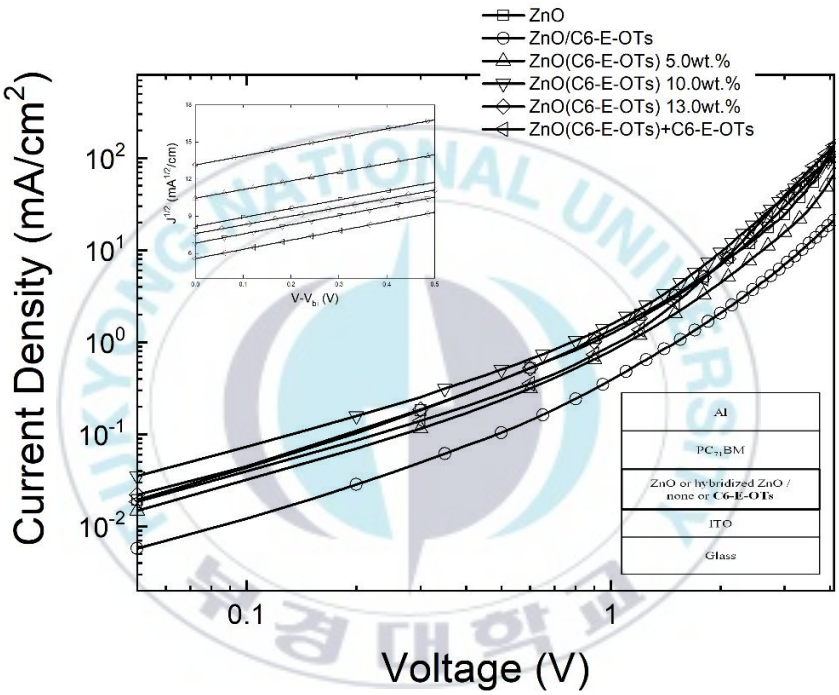

FigureⅢ-15 Current density as a function of voltage curves of electron-only device with $PC_{71}BM$ (V, applied voltage; V_{bi}, built-in voltage).

In order to understand the effect of **C6-E-OTs** on the charge transporting and collection properties, we investigated the photocurrent density (J_{ph}) as a function of the effective voltage (V_{eff}). Here, the J_{ph} and V_{eff} were defined by J_L(measured current density under illumination) $-J_D$ (measured current density in dark condition) and V_0 (voltage at J_{ph} = 0) $-V_a$ (applied voltage), respectively. As shown in **FigureⅢ-16**, the log (J_{ph}) showed a linear relationship to the log (V_{eff}) at a low V_{eff} range and eventually saturated at a high V_{eff} value region. Noticeably, the point of V_{eff} reached at saturated photocurrent is ordered along with the devices based on 10.0 wt. % of **C6-E-OTs** hybridized ZnO and **C6-E-OTs** as the interlayer, 10.0 wt. % of **C6-E-OTs** hybridized ZnO, 5 nm of **C6-E-OTs** as the interlayer on ZnO, 13.0 wt. % of **C6-E-OTs** hybridized ZnO, 5.0 wt. % of **C6-E-OTs** hybridized ZnO, ZnO layer without **C6-E-OTs**. This is strongly related to the trend of the J_{sc} and the PCE of the devices. The maximum exciton generation rate (G_{max}) depends on the absorption of light on the active layer [46] and is determined by $J_{ph}/q \times L$, where q is the electron charge and L is the thickness of the active layer. The G_{max} at the point of saturated current (J_{sat}) of the devices based on ZnO without **C6-E-OTs**, ZnO/**C6-E-OTs** as the interlayer, 5.0 wt. % of **C6-E-OTs** hybridized ZnO, 10.0 wt. % of **C6-E-OTs** hybridized ZnO, 13.0 wt. % of **C6-E-OTs** hybridized ZnO, and 10.0 wt. % of **C6-E-OTs** hybridized ZnO and **C6-E-OTs** as the interlayer were 1.45×10^{28}, 1.59×10^{28}, 1.47×10^{28}, 1.64×10^{28}, 1.54×10^{28}, and 1.64×10^{28} m^3 s^{-1}, respectively. In addition, the carrier transporting and collecting probability at the point of saturated current was estimated from the ratio of J_{ph}/J_{sat} at any V_{eff} (**FigureⅢ-17**) of the devices based on ZnO without **C6-E-OTs**, ZnO/**C6-E-OTs** as the interlayer, 5.0 wt. % of **C6-E-OTs** hybridized ZnO, 10.0 wt. % of **C6-E-OTs** hybridized ZnO, 13.0 wt. % of **C6-E-OTs** hybridized ZnO, and 10.0 wt. % of **C6-E-OTs** hybridized ZnO and **C6-E-OTs** as the interlayer at the J_{sc} condition were 96.0 %, 96.7 %, 96.3 %, 97.1 %, 96.5 %, 97.4 %, respectively. The point of V_{eff} reached at saturated photocurrent, the G_{max}, and the carrier transporting and collecting probability are strongly related to the trend of the J_{sc}

values. These values reveal that the devices with the **C6-E-OTs** exhibited decreased charge recombination and increased charge collection capability at the interfaces.

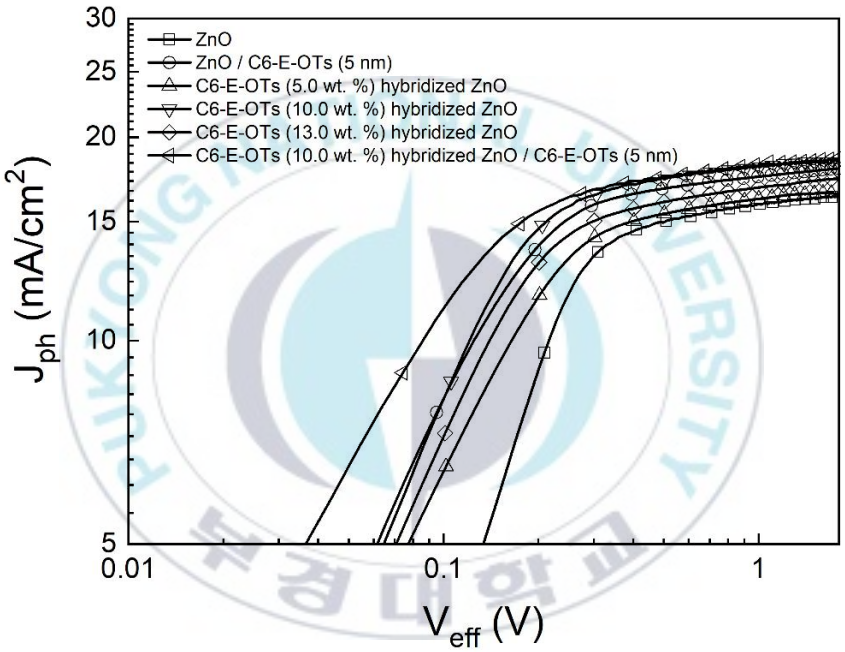

FigureⅢ-16 Photocurrent (J_{ph}) density versus effective voltage (V_{eff}) plots of the devices.

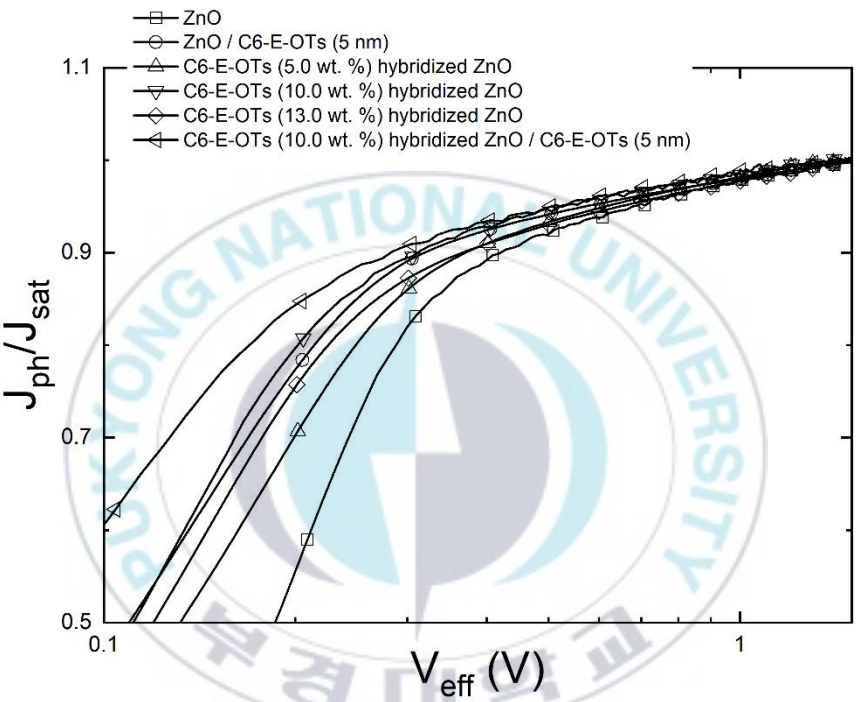

FigureⅢ-17 J_{ph}/J_{sat} versus effective voltage (V_{eff}) plots of the devices.

TableⅢ-4 Photovoltaic parameters of iPSCs based on **C6-E-OTs** with PTB7:$PC_{71}BM$ as the active layer showing the best PCE. The averages are in parentheses.

ETL	J_{SC} (mA/cm^2)	V_{OC} (V)	FF (%)	PCE (%)	R_S[a] (Ω·cm^2)
ZnO	16.0 (15.9)	0.72 (0.72)	65.6 (65.4)	7.6 (7.5)	3.1
ZnO/**C6-E-OTs** (5 nm)	17.3 (17.5)	0.72 (0.71)	68.0 (66.9)	8.5 (8.3)	1.9
C6-E-OTs (5.0 wt. %) hybridized ZnO	16.1 (16.2)	0.73 (0.72)	67.6 (67.3)	8.0 (7.9)	1.9
C6-E-OTs (10.0 wt. %) hybridized ZnO	17.6 (17.6)	0.74 (0.73)	67.6 (67.1)	8.8 (8.7)	2.1
C6-E-OTs (13.0 wt. %) hybridized ZnO	16.6 (16.7)	0.72 (0.72)	66.9 (66.4)	8.0 (8.0)	2.9
C6-E-OTs (10.0 wt. %) hybridized ZnO/ **C6-E-OTs** (5 nm)	17.9 (17.9)	0.73 (0.73)	67.9 (67.8)	8.9 (8.8)	2.8

[a]series resistance are calculated from the device showing the best PCE.

TableⅢ-2 Photovoltaic parameters of iPSCs based on **C6-E-OTs** with PTB7-Th:$PC_{71}BM$ as the active layer showing the best PCE. The averages are in parentheses.

ETL	J_{SC} (mA/cm^2)	V_{OC} (V)	FF (%)	PCE (%)	R_S (Ω·cm^2)
ZnO	15.6 (15.4)	0.80 (0.80)	64.2 (64.4)	8.0 (8.0)	-
C6-E-OTs (10.0 wt. %) hybridized ZnO/ C6-E-OTs (5 nm)	17.9 (17.8)	0.81 (0.81)	65.0 (64.0)	9.4 (9.2)	-

TableⅢ-3 Photovoltaic parameters of iPSCs based on **C6-E-Br** with PTB7:$PC_{71}BM$ as the active layer showing the best PCE. The averages are in parentheses.

ETL	J_{SC} (mA/cm^2)	V_{OC} (V)	FF (%)	PCE (%)	R_S (Ω·cm^2)
ZnO	16.0 (15.9)	0.72 (0.72)	65.6 (65.4)	7.6 (7.5)	3.1
C6-E-Br (5.0 wt. %) hybridized ZnO	15.9 (16.0)	0.72 (0.72)	66.6 (65.9)	7.6 (7.6)	3.2
C6-E-Br (10.0 wt. %) hybridized ZnO	17.0 (16.7)	0.71 (0.71)	66.6 (65.8)	8.0 (7.8)	2.7
C6-E-Br (10.0 wt. %) hybridized ZnO/ C6-E-Br (5 nm)	17.2 (16.9)	0.73 (0.73)	66.1 (66.5)	8.3 (8.2)	2.5

Ⅲ-iv Conclusion

Small-molecule electrolyte, N^1,N^6-bis(2-hydroxyethyl)-N^1,N^1,N^6,N^6-tetramethylhexane-1,6-diaminium bis(4-methylbenzenesulfonate) (**C6-E-OTs**), has been successfully synthesized. **C6-E-OTs** hybridized ZnO layer enhances the PCE up to 8.8 %. The device can be further improved by simultaneously using the **C6-E-OTs** hybridized ZnO layer and a 5 nm thick **C6-E-OTs** as the interlayer simultaneously. The synergy effect of hybridization and interlayer enhanced the PCE of the device to 8.9 % (J_{sc} = 17.9 mA/cm^2, V_{oc} = 0.73 V, FF = 67.9 %), which is a 17.1 % increase in comparison with the device based on ZnO. Moreover, the PCE of the devices based on **C6-E-OTs** is superior to the devices based on **C6-E-Br**. This is due to that a larger counter anion induces a larger interface dipole. The main contribution for enhancing the PCE of the device was improved the J_{sc}, which resulted from the reduction of energy offset at the cathode interface. Thus, the hybridized ZnO layer process can overcome the limitation faced by the thickness tolerance of the interlayer.

References

[1] Rasool, S. Ichtiaque, and Stephen H. Schneider. "Atmospheric carbon dioxide and aerosols: Effects of large increases on global climate." *Science* 173, 3992 (1971) 138-141.

[2] Liang, Yongye, et al. "For the bright future—bulk heterojunction polymer solar cells with power conversion efficiency of 7.4%." Advanced materials 22, 20 (2010) E135-E138.

[3] Louwen, Atse, et al. "Life□cycle greenhouse gas emissions and energy payback time of current and prospective silicon heterojunction solar cell designs." Progress in Photovoltaics: Research and Applications 23, 10 (2015) 1406-1428.

[4] Lewis, Nathan S. "Toward cost-effective solar energy use." science 315, 5813 (2007) 798-801.

[5] Carlson, David E., and Cristopher R. Wronski. "Amorphous silicon solar cell." Applied Physics Letters 28, 11 (1976) 671-673.

[6] Zhang, Hao, et al. "Over 14% efficiency in organic solar cells enabled by chlorinated nonfullerene small□molecule acceptors." Advanced materials 30, 28 (2018) 1800613.

[7] Park, Song Yi, et al. "Non-halogenated diphenyl-chalcogenide solvent processing additives for high-performance polymer bulk-heterojunction solar cells." RSC advances 8, 69 (2018) 39777-39783.

[8] Zhou, Huanping, et al. "Interface engineering of highly efficient perovskite solar cells." Science 345, 6196 (2014) 542-546.

[9] Semonin, Octavi E., et al. "Peak external photocurrent quantum efficiency exceeding 100% via MEG in a quantum dot solar cell." Science 334, 6062 (2011) 1530-1533.

[10] Mathew, Simon, et al. "Dye-sensitized solar cells with 13% efficiency achieved through the molecular engineering of porphyrin sensitizers." Nature chemistry 6, 3 (2014) 242-247.

[11] Hong, Ling, et al. "Eco□compatible solvent□processed organic photovoltaic cells with over 16% efficiency." Advanced materials 31, 39 (2019) 1903441.

[12] Zhang, Shaoqing, et al. "Over 14% efficiency in polymer solar cells enabled by a chlorinated polymer donor." Advanced Materials 30, 20 (2018) 1800868.

[13] Krebs, Frederik C., Suren A. Gevorgyan, and Jan Alstrup. "A roll-to-roll process to flexible polymer solar cells: model studies, manufacture and operational stability studies." Journal of Materials Chemistry 19, 30 (2009) 5442-5451.

[14] Krebs, Frederik C., Thomas Tromholt, and Mikkel Jørgensen. "Upscaling of polymer solar cell fabrication using full roll-to-roll processing." Nanoscale 2, 6 (2010) 873-886.

[15] Bencheikh, Fatima, et al. "Study of optical properties and molecular aggregation of conjugated low band gap copolymers: PTB7 and PTB7-Th." The Journal of Physical Chemistry C 119, 43 (2015) 24643-24648.

[16] Duan, Leiping, et al. "Progress in non-fullerene acceptor based organic solar cells." Solar Energy Materials and Solar Cells 193 (2019) 22-65.

[17] Feron, Krishna, et al. "Organic solar cells: understanding the role of Förster resonance energy transfer." International journal of molecular sciences 13, 12 (2012) 17019-17047.

[18] Grancini, Giulia, et al. "Hot exciton dissociation in polymer solar cells." Nature materials 12, 1 (2013) 29-33.

[19] Shaw, Paul E., Arvydas Ruseckas, and Ifor DW Samuel. "Exciton diffusion measurements in poly (3□hexylthiophene)." Advanced Materials 20, 18 (2008) 3516-3520.

[20] McNeill, Christopher R., and Neil C. Greenham. "Conjugated□polymer blends for optoelectronics." Advanced Materials 21, 38□39 (2009) 3840-3850.

[21] Chen, Hsiang-Yu, et al. "Polymer solar cells with enhanced open-circuit

voltage and efficiency." Nature photonics 3, 11 (2009) 649-653.

[22] Hau, Steven K., Hin-Lap Yip, and Alex K-Y. Jen. "A review on the development of the inverted polymer solar cell architecture." Polymer Reviews 50, 4 (2010) 474-510.

[23] Liu, Huimin, et al. "Polyfluorene electrolytes interfacial layer for efficient polymer solar cells: controllably interfacial dipoles by regulation of polar groups." ACS Applied Materials & Interfaces 8, 15 (2016) 9821-9828.

[24] Wang, Fuzhi, Zhan'ao Tan, and Yongfang Li. "Solution-processable metal oxides/chelates as electrode buffer layers for efficient and stable polymer solar cells." Energy & Environmental Science 8, 4 (2015) 1059-1091.

[25] Tung, R. T. "Schottky-barrier formation at single-crystal metal-semiconductor interfaces." Physical review letters 52, 6 (1984) 461.

[26] Tung, Raymond T. "The physics and chemistry of the Schottky barrier height." Applied Physics Reviews 1, 1 (2014) 011304.

[27] Shen, Yulong, et al. "How to make ohmic contacts to organic semiconductors." ChemPhysChem 5, 1 (2004) 16-25.

[28] Chen, Song, et al. "Metal oxides for interface engineering in polymer solar cells." Journal of Materials Chemistry 22, 46 (2012) 24202-24212.

[29] Cai, Yunhao, et al. "Novel nonconjugated polymer as cathode buffer layer for efficient organic solar cells." ACS applied materials & interfaces 10, 28 (2018) 24082-24089.

[30] Li, Yaru, et al. "Electrolytes as Cathode Interlayers in Inverted Organic Solar Cells: Influence of the Cations on Bias-Dependent Performance." ACS Applied Materials & Interfaces 9, 9 (2017) 8426-8431.

[31] Barnham, K. W. J., et al. "Short□circuit current and energy efficiency enhancement in a low□dimensional structure photovoltaic device." Applied physics letters 59, 1 (1991) 135-137.

[32] Padilla, M., et al. "Short-circuit current density mapping for solar cells." Solar energy materials and solar cells 120 (2014) 282-288.

[33] Chen, Hsiang-Yu, et al. "Polymer solar cells with enhanced open-circuit

voltage and efficiency." Nature photonics 3, 11 (2009) 649-653.

[34] Shaheen, Sean E., et al. "2.5% efficient organic plastic solar cells." Applied Physics Letters 78, 6 (2001) 841-843.

[35] He, Chao, et al. "Origin of the enhanced open-circuit voltage in polymer solar cells via interfacial modification using conjugated polyelectrolytes." Journal of Materials Chemistry 20, 13 (2010) 2617-2622.

[36] Noer, N. M., et al. "Employing Successive Ionic Layer Adsorption and Reaction (SILAR) Method on the Fabrication of Cu_3BiS_3-Semiconductor-Sensitized Solar Cells." Journal of Physics: Conference Series. Vol. 1542. No. 1. IOP Publishing, 2020.

[37] Randall, J. F., and J. Jacot. "Is AM1. 5 applicable in practice? Modelling eight photovoltaic materials with respect to light intensity and two spectra." Renewable Energy 28, 12 (2003) 1851-1864.

[38] Chen, Yen-Chia, et al. "Surfactant-enriched ZnO surface via sol–gel process for the efficient inverted polymer solar cell." ACS applied materials & interfaces 10, 31 (2018) 26805-26811.

[39] Guo, Xuewen, et al. "Novel small-molecule zwitterionic electrolyte with ultralow work function as cathode modifier for inverted polymer solar cells." Organic Electronics 59 (2018) 15-20.

[40] He, Zhicai, et al. "Enhanced power-conversion efficiency in polymer solar cells using an inverted device structure." Nature photonics 6, 9 (2012) 591-595.

[41] You, Hailong, et al. "Low Temperature Aqueous Solution-Processed ZnO and Polyethylenimine Ethoxylated Cathode Buffer Bilayer for High Performance Flexible Inverted Organic Solar Cells." Energies 10, 4 (2017) 494.

[42] Zhou, Dan, et al. "A green route to a novel hyperbranched electrolyte interlayer for nonfullerene polymer solar cells with over 11% efficiency." Chemical Communications 54, 5 (2018) 563-566.

[43] Wu, Zhihong, et al. "n-Type water/alcohol-soluble naphthalene diimide-

based conjugated polymers for high-performance polymer solar cells." Journal of the American Chemical Society 138, 6 (2016) 2004-2013.

[44] Dagar, Janardan, et al. "Coating ZnO nanoparticle films with DNA nanolayers for enhancing the electron extracting properties and performance of polymer solar cells." Nanoscale 9, 48 (2017) 19031-19038.

[45] Duan, Tainan, et al. "Simple organic donors based on halogenated oligothiophenes for all small molecule solar cells with efficiency over 11%." Journal of Materials Chemistry A 8, 12 (2020) 5843-5847.

[46] Tran, Van-Huong, et al. "Enhancing device performance of inverted organic solar cells with SnO_2/Cs_2CO_3 as dual electron transport layers." Organic Electronics 68 (2019) 85-95.

[47] Yu, Huangzhong, Xinxin Huang, and Chengwen Huang. "PEIE doped ZnO as a tunable cathode interlayer for efficient polymer solar cells." Applied Surface Science 470 (2019) 318-330.

[48] Hu, Zhicheng, et al. "Quaternisation-polymerized N-type polyelectrolytes: synthesis, characterisation and application in high-performance polymer solar cells." Materials Horizons 4, 1 (2017) 88-97.

Acknowledgement

먼저 많은 것을 배울 수 있게 해주신 **김주현 교수님**께 감사드립니다. 교수님 덕분에 3년 동안 실험실에서 다양한 경험을 해볼 수 있었고 성장할 수 있었습니다. 그리고 학부 때부터 많은 가르침을 주시고 좋은 길로 인도해주셨던 고분자공학과의 모든 교수님들께도 감사드립니다.

하루도 빠짐없이 밝은 에너지와 상냥한 미소로 대해주신 **지현쌤**, **다빈쌤**, 늘 잘챙겨주셔서 감사합니다. 쌤들 덕분에 과사에서 힐링 많이 했고 힘 많이 얻어 갔습니다. 쌤들 최고!

그리고 OOM 식구들. 디바이스방에서 같이 고생하고 많은 이야기를 나눴던 **호철선배**, **준호선배**, 울 선배님들 항상 좋은 일만 있기를 바랍니다. **사브리나**, **동환이**, **아날리아**, **라마**는 좀 더 고생하고 힘내소ㅎㅎ OOM 사람들 다들 항상 행복하고 건강 잘 챙겨(요).

좋은 추억 많이 만들어준 잊지 못 할 친구들, **Sabrina**, **Pujil**, **Molly**, 그리고 같이 놀면 재밌는, 놀 줄 아는 친구들, **Ratna**, **Arda**. 모두 고맙고 사랑한다. **Ratna**, **Arda**는 서울에서 만나서 놀고 **Sabrina**, **Pujil**, **Molly**는 발리에서 만나!

그리고 내가 행복할 수 있는 이유인 나의 모든 **친구들**, 항상 나를 응원해주고 힘이 되어주는 **가족들**도, 정말 많이 사랑합니다.

끝으로 많은 시간 함께 한 모든 분들께 다시 한 번 감사드립니다.

2021년 02월

정미진 올림